Model Driven Paediatric European Digital Repository

Call identifier: FP7-ICT-2011-9 **Grant agreement no**: 600932

Thematic Priority: ICT - ICT-2011.5.2: Virtual Physiological Human

Deliverable 10.4

Biomechanical simulation based on image based modelling and gait analysis

Due date of delivery: M36 – February 2016

Actual submission date: M37 – March 2016

Start of the project: 1st March 2013

Ending Date: 28th February 2017

Partner responsible for this deliverable: USFD

Dissemination Level: Reserved

Document Classification

Title	Biomechanical simulation based on image based modelling and gait analysis
Deliverable	D 10.4
Reporting Period	M24-M36
Authors	USFD/FhG/IGG/OPBG/URLS
Work Package	WP 10
Security	Reserved
Nature	Report
Keyword(s)	Juvenile Idiopathic Arthritis, Musculoskeletal, Ankle, Modelling, Gait analysis, MRI

List of Contributors

Name	**Affiliation**
Luca Modenese	USFD
Erica Montefiori	USFD
Claudia Mazzà	USFD
Marco Viceconti	USFD
Roberto Di Marco	URLS
Paolo Cappa	URLS
Stefan Wesarg	FhG
Anqi Wang	FhG
Pieter van Dijkhuizen	IGG
Clara Malattia	IGG
Anna Ronchetti	IGG
Maurizio Petrarca	OPBG
Silvia Magni Manzoni	OPBG
Laura Tanturri de Horatio	OPBG

List of reviewers

Name	**Affiliation**
Frans Steenbrink	Motek
Bruno Dallapiccola	OPBG

Abbreviations

USFD	The University of Sheffield
FhG	Fraunhofer Institute
IGG	Istituto Giannina Gaslini
OPBG	Ospedale Pediatrico Bambino Gesù
UMCU	Universitair Medisch Centrum Utrecht
CGA	Clinical gait analysis
MRI	Magnetic resonance imaging
EMG	Electromyography
SSM	Statistical shape modelling
ROM	Range of motion
mOFM	Modified Oxford Foot Model
LFM	Linear Fit Method
IC	Initial Contact
TO	Toe-off
MAD	Median Absolute Deviation
MD	Maximum difference

Table of Contents

Summary

The goal of this work package is to build patient-specific biomechanical models of the musculoskeletal system of children affected by juvenile idiopathic arthritis. These models, built and driven using magnetic resonance images (MRI) and gait analysis, are used to run biomechanical simulation of a child's gait, and yield estimates of muscle forces and joint contact forces. In the framework of this project, these quantities will be used as biomarkers for the assessment of the pathology progression. In this deliverable we describe the methodologies that have been developed and validated within WP10 to build articulated geometrical models of both the ankles and lower limbs. The ankle models are built using the foot and ankle MRIs acquired at month 0 and month 12. The relevant computational pipeline presented in a previous deliverable has now been refined to account for the results of an analysis of its reliability and sensitivity. The lower limb models are built using the lower limb MRI collected at month 6. A pipeline for the creation of these models has now been implemented which also includes the definition of the procedures needed to combine these models with those created at month 0 and month 12. Last, the steps required to simulate patient gait at the different time points have been defined and the results of the simulations performed on the one complete dataset available are presented.

1 Modelling data

1.1 Patient recruitment and data collection

The children affected by juvenile idiopathic arthritis recruited for modelling purposes in W10 have their ankle joints assessed 3 times, at 6-month intervals. The patients' ankles or lower limb are scanned using magnetic resonance imaging (MRI) and they undergo a clinical gait analysis (CGA) (Table 1 summarises the data collection procedure). The imaging and gait analysis protocols, developed in collaboration between the clinical and modelling work packages and fully described in Appendices A and B of deliverable D10.1 respectively, have been consistently adopted in the clinical data collection.

Table 1: Summary of data measured at the three time points considered in the project.

Time after recruitment	Data collection relevant for modelling
Month 0	Ankles MRI (both ankles scanned at the same time, also in patients with unilateral ankle involvement) Gait analysis
Month 6	Lower limbs MRI Gait analysis
Month 12	Ankles MRI Gait analysis

Previous deliverables from the clinical partners (D5.1 and D5.3) presented the recruitment criteria for the early-onset and long-term patients respectively: Only patients between five and sixteen years of age were considered for the anatomical and biomechanical modelling part of the study for practical reasons related to the data acquisition (immobility during MRI scanning and compliance during the gait analysis). An update on the patient recruitment status is provided in the following sections.

In all three clinical centres combined, 170 patients have been enrolled. Enrolment closed in December 2015. At the time of writing, data for the first 165 enrolled patients was available. Numbers and percentages are based on those patients only. Overall, 71 (43%) patients had clinical ankle involvement at baseline. However, many of these were too young (less than six years old) to perform the MRI and CGA. Moreover, patients seen at UMCU did not perform CGA due to insuperable differences in the equipment used at UMCU on the one hand, and IGG and OPBG on the other. Therefore, 14 new-onset patients were included to perform MRI of the affected and contralateral ankle at baseline. Of these, 12 patients also performed CGA as well with the difference of two patients being due to the fact that these patients performed an MRI, but not a CGA, at UMCU.

As discussed in previous deliverables, because the number of participants eligible to perform MRI and CGA remained lower than expected, it was decided to allow the inclusion of patients with long-term ankle involvement as well, solely for the purpose of constructing a biomechanical ankle model. Of these patients, 14 could be enrolled at IGG and OPBG combined, all of whom performed the MRI and CGA at baseline.

The follow up of the enrolled patients was according to the protocol detailed in Table 1. Unfortunately, three patients refused further participation after the baseline examinations, mainly due to difficulties in establishing appointments. For the remaining patients, follow up MRIs and CGAs have been performed, as reported in Table 2. These patients will continue their follow up in the remaining study period.

Table 2: MRI and CGA data collection.

[a] Ankle MRI at month 0, 12 and 24 and a lower limb MRI at month 6. See Table 1.

	New onset		**Long-term**		**Total**	
	MRI[a]	**CGA**	**MRI[a]**	**CGA**	**MRI**	**CGA**
Month 0	14	12	12	12	26	24
Month 6	9	9	10	10	19	19
Month 12	7	6	0	0	7	6
Month 24	1	N/A	0	N/A	1	N/A

1.2 Data quality control

A procedure for quality control, agreed between the clinical and modelling partners, has been applied to evaluate all of the acquired datasets with the majority of the follow-up data has satisfying the required standards (Table 3). Most of the issues observed were related to the EMG recordings due to instrumentation failure in the IGG gait laboratory (summer 2015) and noisy gait trials in the OPBG gait laboratory. These EMG signals are being collected as an indirect tool for the validation of the estimated muscle activations. This validation will be performed using the other available datasets, which are numerous enough to this purpose. Other less frequent issues of different kinds have also been observed and are identified in Table2 where the modelling possibility is consequently considered “limited”. However, the modelling procedure developed so far has been developed with the intention of trying to model as many patients as possible, by being robust and flexible enough to deal with incomplete or noisy datasets.

Table 3: Status of the data collection quality checks, in terms of the adherence to the described imaging and gait analysis protocol (data is displayed in order of collection from oldest to most recent). *some markers are missing (both MRI and gait analysis), ** to be relabelled (CGA) or noisy (CGA and MRI), + incomplete or only one foot in MRI scan, ++EMG missing or corrupted.

Patient	Month 0			Month 6			Month 12		
	MRI	CGA	Modelling possibility	MRI	CGA	Modelling possibility	MRI	CGA	Modelling possibility
IGG-GC-15052004	*No; test MR only*	*No; test MRI only*	*No*						
IGG-JL-16031998	*No+*	*No**	*Very limited*						
IGG-MG-17111999	No; incorrect protocol	No; 2 month gap	No	Yes	Yes	Yes	Yes	Yes	Yes
IGG-GG-23052000	No; broken MRI	N/A	No						
IGG-AP-06122004	No*	Yes	Very limited	Yes	Yes	Yes	Yes	Yes++	Yes
IGG-CS-26061999	No*	Yes	Very limited	Yes**	Yes	Limited			
IGG-DO-02042001	No*	Yes	Very limited	Yes+	Yes	Limited	Yes+	Yes	Limited
IGG-NC-06071998	No*	Yes	Very limited						
IGG-RF-25122000	No*	Yes	Limited	Yes	Yes	Yes	Yes	Yes**	Yes
IGG-ET-04041997	Yes	Yes	Yes	Yes	Yes++	Limited			
IGG-EP-26072004	Yes	Yes	Yes						
IGG-FA-14111998	Yes	Yes	Yes	Yes*	Yes**	Limited			
IGG-MM-19102004	Yes	Yes	Yes	Yes	Yes**	Yes	Yes	Yes++	Limited
IGG-ER-11012005	Yes	Yes	Yes	Yes	Yes	Yes			
IGG-VA-03112006	Yes	Yes**	Yes	Yes	Yes++	Limited			
OPBG-GC-20082005	No+	No*	Very limited	No*	Yes	Very limited	Yes	Yes++	Yes
OPBG-AA-23012007	Yes	No*,++	Very limited	Yes	Yes**	Yes			
OPBG-LV-05072001	Yes	Yes	Yes	Yes	Yes	Yes			
OPBG-MG-07012001	Yes	No++	Very limited	No*	Yes**	Very limited	Yes+	Yes++	Limited
OPBG-MT-21082001	Yes	Yes	Yes	Yes	Yes	Yes	Yes+	Yes++	Limited
OPBG-FZ-28102007	Yes	Yes	Yes	No*	N/A	Very Limited			
OPBG-SL-16082007	Yes	Yes	Yes						
OPBG-VF-08092001	Yes	Yes**	Yes	Yes	Yes++	Yes			
OPBG-CR-30042008	Yes	Yes	Yes	No+	Yes++	Limited			
OPBG-RD-1611205	Yes	Yes	Yes						
OPBG-AC-08122005	Yes	Not received	N/A						

2 Data processing update

The early stages of the project have focused on establishing a modelling pipeline to allow the conversion of the raw data into models to be used for extracting relevant biomarkers. This process has involved three research groups working on; definition of the kinematics models and protocols (URLS), extraction of the geometrical articulated models from the MRI images via semi-automated segmentation software (FhG), and musculoskeletal modelling (USFD). This section presents an update on the progress of each group with respect to D10.1.

2.1 URLS update

For the purpose of this project, clinical and technical partners worked together to select the marker placement protocol that seemed to yield the most reliable results among those proposed in literature. Indeed, clinical decision-making and assessment of JIA patients might largely benefit from objective measurement of foot kinematics according to multi-segmental models. Based on a review of the literature, the modified Oxford Foot Model, mOFM (Stebbins et al., 2006), was chosen to assess the gait of JIA patients enrolled in this project and it defines the following joint angles:

- Thigh relative to pelvis;
- Tibia relative to thigh;
- Hindfoot relative to tibia;
- Forefoot relative to hindfoot;
- Forefoot relative to tibia;
- Hallux relative to forefoot.

Although widely used, the validation of this model is limited and clinical utility has been somewhat questioned (Baker and Robb, 2006). Indeed, foot kinematics is expected to be less repeatable than kinematics of the other lower limb joints due to small palpated bony prominences and small marker clusters (Caravaggi et al., 2011). As a result of these concerns, repeatability and reproducibility analyses of the mOFM outcomes for the foot-ankle complex, were carried out by URLS and USFD.

Due to the limitations imposed by the MD-Paedigree study ethical approval, the analyses were performed on *ad hoc* data gathered from a healthy adult population recruited at the University of Sheffield, which granted ethical approval to this study. Thirteen healthy subjects were recruited for the study (ten males, age: 27.0 ± 1.9 years, height: 1.83 ± 0.08 m, foot length: 28.5 ± 1.0 cm). Exclusion criteria were self-reported musculoskeletal pain or impairments. Prior to the data collection, all subjects read and signed a consent form. Marker trajectories were collected with a 10-camera stereophotogrammetric system (100 Hz, Vicon Nexus 1.8.5, Vicon Motion System Ltd – Oxford, UK). Labelling, gait cycle-event saving, gap filling, and filtering were conducted within Nexus with the C3D files then exported for post-processing in MATLAB (R2015b, The MathWorks, Inc. – Natick, MA, USA). Data were smoothed with Woltring spline routine, size 30

(Woltring, 1986). The local coordinate systems for each segment were defined according to the description in the paper; in particular, the option 5 was declared as the most repeatable configuration (static calibration and dynamic tracking of the hindfoot do not consider the wand marker). The joint kinematics were then computed according to a least square fitting approach (Soderkvist and Wedin, 1993).

2.1.1 Within- and between-subject repeatability analyses

A trained operator placed the marker-set on each of the subjects who were then asked to walk barefoot at a self-selected speed on a treadmill (ADAL3D-F, TECMACHINE HEF Groupe – Andreziéux Bouthéon, France) – walking speed was 0.82±0.15 m/s. This condition is considered the most controlled and produces the least variation in the relevant joint kinematics. The operator also recorded the relevant anthropometric measurements. Two sessions of data collection were carried out one month apart, with the same operator replacing the markers. A total of five right strides were recorded from each session for analysis.

Waveform similarity was assessed using the Linear Fit Method (LFM) (Iosa et al., 2014). This method was chosen rather than the more commonly considered Coefficient of Multiple Correlation (Kadaba et al., 1989) since it is intrinsically not affected by the presence of possible spikes, outliers or offset, which, conversely, can cause an undesired decrease of the Coefficient of Multiple Correlation (Røislien et al., 2012). The method is based on applying a point-by-point linear fitting to dataset P_a and reference, which is equivalent to solving a least square problem on the residuals between P_a and the linear regression line Y_a defined as follows:

$$Y_a = a_0 + a_1 \cdot P_{ref} \qquad \text{(Eq. 1)}$$

The coefficients are then interpretable as the angular coefficient (a_1) and the intercept (a_0) of the regression line, where:

$$\begin{aligned} a_1 &= \frac{\sum_{i=1}^{n}\left(P_{ref}(i)-\overline{P}_{ref}\right)\cdot\left(P_a(i)-\overline{P}_a\right)}{\sum_{i=1}^{n}\left(P_a(i)-\overline{P}_a\right)^2}, \\ a_0 &= \overline{P}_a - a_1 \cdot \overline{P}_{ref}, \\ R^2 &= \frac{\sum_{i=1}^{n}\left(a_0 + a_1 \cdot P_{ref}(i)-\overline{P}_a\right)^2}{\sum_{i=1}^{n}\left(P_a(i)-\overline{P}_a\right)^2}. \end{aligned} \qquad \text{(Eq. 2)}$$

In this study, the dataset P_a and the reference P_{ref} were composed by 101 samples (i.e., $n = 101$).

The three coefficients yielded can be interpreted as follows:

- a_1 is the scaling factor between the comparing curves and the similarity index (the closer to 1, the more similar the curves);
- a_0 measures the shift between the curves, quantifying the offset;
- R^2 validates the linear relationship between the curves and measures their correlation (the closer to 1, the stronger the linear model is).

In the case of the within-subject, the *i*-th kinematic curve at the *j*-th gait cycle was compared to the same kinematics averaged among the five strides and the two sessions.

Repeatability was assessed by considering the values of the sagittal joint angles with both the LFM coefficients on the entire kinematic curves, and the joint angle at initial contact (IC) and toe-off (TO) as relevant summary metrics (Wilken et al., 2012). The median absolute deviation (MAD) and the maximum difference (MD) were subsequently calculated on those metrics. The former is a variability index reported to be robust to the outliers, whereas the latter measures the differences obtained in the worst case (Benedetti et al., 2013).

2.1.2 Between-operator reproducibility analysis

A subset of three male subjects (age: 25.7 ± 2.3 years, height: 1.84 ± 0.08 m, foot length: 28.7 ± 0.2 cm), randomly selected among those recruited, was considered for this analysis. Three trained operators repeated the marker placement and measurement of the relevant anthropometric parameters three times. Subjects walked barefoot on the treadmill at a self-selected speed (walking speed: 0.97 ± 0.24 m/s). Five right strides were isolated for the analysis. The agreement between the kinematic curves was tested using the LFM, and the same summary metrics considered in the within- and between-subject analyses were used to calculate median absolute deviation (MAD) and maximum difference (MD).

2.1.3 Results

Table 4 shows the results obtained for both the repeatability and reproducibility analyses. The within-subject analysis provided information on the effects of the marker repositioning, while controlling for the possible differences due to both the between-strides and between-sessions variabilities. Although the mOFM does not require any reference posture to define the joint angles, the offset parameter a_0 and its standard deviation of the relevant kinematics displayed values between 1° and 4°. Correlations were always higher than 0.91, and the averaged similarity a_1 was always equal to 1 with the highest standard deviation equal to 0.15. This leads to the conclusion that the mOFM produces repeatable within-subjects results. Contrastingly, the between-subject repeatability analysis highlighted some critical issues concerning the clinical meaningfulness of normative bands. Particular care should be taken when utilising HF-Tib, and Hal-FF due to the large between-subject variability displayed at the lower values for all considered indices. Reported LFM coefficients and particularly the offset parameter a_0 showed that the effect of the marker repositioning on

the same subject (repeatability) produces a similar effect to the repositioning performed by different operators (reproducibility). Although a bias might be introduced by the different sample sizes considered for these analyses, the equivalence of the two effects suggests that the variability of the foot motion is higher than any other source of variability.

Table 4: Range of Motion (ROM), Linear Fitting Method (LFM) coefficients, Median Absolute Deviation (MAD) and Maximum Difference (MD) at initial contact (IC) and toe-off (TO) obtained from the within- and between-subject repeatability and from the between-operator reproducibility analyses in the walking condition. Segment names are abbreviated as follows: Tibia (Tib), hindfoot (HF), forefoot (FF), hallux (Hal).

		Joints	ROM (°)	LFM coefficients			MAD (°)		MD (°)	
				a_1	a_0 (°)	R^2	IC	TO	IC	TO
Repeatability	*Within subjects*	*Knee*	52 ± 7	1.00 ± 0.06	0 ± 3	0.97 ± 0.04	1 ± 1	1 ± 1	4 ± 2	6 ± 2
		HF-Tib	16 ± 3	1.00 ± 0.11	0 ± 1	0.91 ± 0.09	1 ± 0	1 ± 0	2 ± 1	4 ± 2
		FF-HF	11 ± 2	1.00 ± 0.13	0 ± 1	0.94 ± 0.06	1 ± 0	0 ± 0	2 ± 1	2 ± 1
		FF-Tib	26 ± 5	1.00 ± 0.09	0 ± 1	0.93 ± 0.08	1 ± 1	1 ± 1	3 ± 1	6 ± 2
		Hal-FF	24 ± 5	1.00 ± 0.15	0 ± 4	0.92 ± 0.08	1 ± 1	1 ± 0	3 ± 1	4 ± 1
	Between subjects	*Knee*	52 ± 7	1.00 ± 0.17	0 ± 6	0.92 ± 0.07	3	5	22	18
		HF-Tib	16 ± 3	1.00 ± 0.25	0 ± 4	0.73 ± 0.16	1	3	13	18
		FF-HF	11 ± 2	1.00 ± 0.21	0 ± 2	0.85 ± 0.10	2	2	8	11
		FF-Tib	26 ± 5	1.00 ± 0.18	0 ± 3	0.78 ± 0.14	4	5	14	22
		Hal-FF	24 ± 5	1.00 ± 0.29	0 ± 7	0.74 ± 0.16	4	5	22	30
Reproducibility	*Between operators*	*Knee*	43 ± 1	1.00 ± 0.09	0 ± 4	0.98 ± 0.01	1 ± 1	2 ± 2	6 ± 3	9 ± 5
		HF-Tib	11 ± 0	1.00 ± 0.12	0 ± 2	0.82 ± 0.09	1 ± 1	1 ± 0	3 ± 1	5 ± 2
		FF-HF	7 ± 0	1.00 ± 0.15	0 ± 2	0.88 ± 0.08	1 ± 1	1 ± 1	6 ± 3	5 ± 2
		FF-Tib	17 ± 0	1.00 ± 0.13	0 ± 4	0.84 ± 0.10	1 ± 1	1 ± 1	7 ± 4	8 ± 4
		Hal-FF	13 ± 2	1.00 ± 0.28	0 ± 7	0.79 ± 0.15	3 ± 2	3 ± 2	11 ± 6	12 ± 5

2.1.4 Conclusion

The model proposed by Stebbins et al. (2006) led to good results in terms of within-subject repeatability. However, the results clearly showed **that it is questionable to assume foot kinematics to be repeatable and hence to rely on normative bands for the clinical assessment of patients**. This is consistent with the approach adopted in MD-Paedigree, where only intra-subject and longitudinal analyses will be performed. Moreover, **these results emphasise the need for an MRI-based definition of the foot and ankle joint axis.**

2.2 FhG update

The statistical shape model (SSM) based approach chosen to produce geometrical models of the lower limb and the specific enhancements for the MD-Paedigree project with respect to its initial development (Steger et al., 2012) were described in Deliverable 10.1.

A challenge for the usage of SSMs for segmentation is the necessity of a sufficiently large set of training data. This means that a significant amount of manually created segmentations is needed as input for the model-training step. Now that data is also available from month 6 and month 12, the processing is extended to

include these as well. The manual segmentation of the bones for creating a sufficient number of training data sets is very time-consuming: it takes up to 30 hours to process one dataset (14 bones and the skin). So far 15 datasets have been produced from which ten are of left feet and five of right feet. By flipping the segmentations of the right feet, we have a total of fifteen datasets for the left foot. These allow us to build a model (Figure 1). The phalanges which were formerly missing due to field-of-view problems are now included in the model, though in a simplified way: They are presented as just one bone each, although they normally consist of 3, respectively of 2 (in case of phalanx I) smaller bones. This simplification was agreed upon to accelerate the manual segmentation process because it does not influence the results of further analysis.

Figure 1: The model for the left foot bone structures from different angles

For model adaptation, i.e. automatic labelling of the anatomical structures, a straightforward gradient-based approach is currently used. At this point the model is manually initialized, i.e. the user has to choose three points in the MR image, namely the centre points of the bones Calcaneus, Tibia and Metatarsal I. The correspondent points of the model are then mapped to the points selected. After this initialization step, the structures are each iteratively shifted towards probable surfaces nearby, represented by high gradient values, which originate from the strong contrast between bones and tissues in MRI-images. The first results of this approach (Figure 2) are promising; however the well-known problem of non-standardized image heterogeneities of MRI has to be solved before further improvements can be made. The lack of a normalized, biologically interpretable intensity range (as in CT images) renders it impossible to have universally applicable model adaptation parameters. The next steps are therefore image intensity normalization and de-noising.

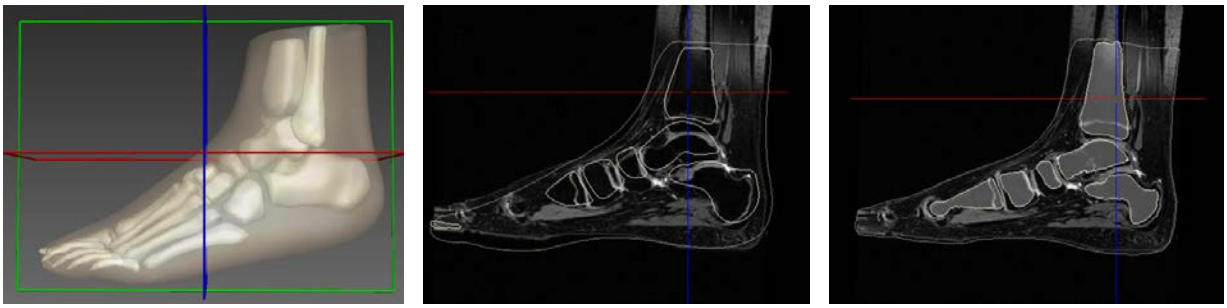

Figure 2: Left: Trained model Middle: Model position after manual initialization Right: Preliminary segmentation result

The lower limb data acquired at month 6 are split into four or five parts consisting of hips, thighs, knees, calves and feet of the respective patient. Since the position of the patient did not change during image acquisition, these images could easily be merged into one volume of the complete lower limbs. The next processing steps are akin to those of the ankle images. After obtaining a sufficient amount of training data a coupled shape model of the limbs will be generated, which will then allow the automated segmentation of further data sets. At this point, 10 patient datasets were manually segmented, each at least containing the structures Femur, Patella, Tibia and Fibula. For six of these datasets, the left and right Illiacus bone and the Sacrum are also segmented. Using this data, a model could be built (Figure 3).

Figure 3: Lower limbs bone model

One problem however arises from the partitioning (Figure 4): Though the image parts are registered, edges remain where image intensities are differently distributed. When applying our gradient based adaptation approach to these images, these edges could be difficult to handle. Also for the lower limbs images, more pre-processing steps are needed to improve the results of the segmentation.

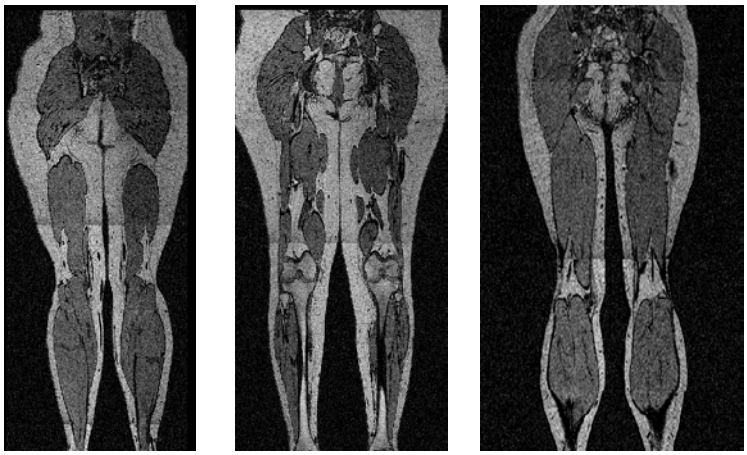

Figure 4: Remaining intensity edges in fused lower limb images

2.3 USFD update

The activities of USFD in the reporting period focused on processing the datasets provided by FhG with the aim of creating patient specific biomechanical models. Table 5 shows a list of all the available datasets with relevant comments on the modelling possibilities. Overall, 6 out of 15 (40%) of the available ankles geometries at month-0, 2 out of 7 (29%) of the available full body geometries at month-6 and 2 out of 2 (100%) at month 12 have been processed so far for modelling purposes.

In particular, in addition to the four patient specific lower limb musculoskeletal models built for D10.1 (3 models of different patients at month-0 and 1 model at month-6), the following personalised musculo-skeletal models are now available for patient IGG-RF, who was the only patient for whom complete datasets including the observations at month 0, 6 and 12 was available at the time of writing:

- A bi-lateral subject-specific model of both limbs, including patient specific feet at month-0
- A bi-lateral subject-specific model of both limbs at month-6
- A bi-lateral subject-specific model of both limbs, including patient specific feet at month-12

Details about the modelling procedures and the relevant results are reported in the following chapters.

Table 5: Status of the data processing. The models included are those that have either: completely adhered to the protocols, been segmented, or have had models created of them. 'STL' refers to the 3D bone and muscle digital representation as extracted from MRI. FhG = Fraunhofer, USFD = Sheffield, * waiting for pelvis segmentation, ** segmented at USFD but to be updated using FhG segmentation.

Patients	Month 0			Month 6			Month 12		
	Modelling possibility	Segmentation	Models	Modelling possibility	Segmentation	Models	Modelling possibility	Segmentation	Models
IGG-GC-15052004	*No*	*Done 1 foot (FhG)*							
IGG-JL-16031998	*Very limited*	*Done 1 foot (USFD)*	*Built*						
IGG-MG-17111999	No			Yes			Yes		
IGG-GG-23052000	No								
IGG-AP-06122004	Very limited	*Done 1 foot (FhG)*	*Built*	Yes	*Done (FhG)*		Yes		
IGG-CS-26061999	Very limited			Limited	*Done (FhG)*				
IGG-DO-02042001	Very limited			Limited	*Done (FhG)*		Limited		
IGG-NC-06071998	Very limited								
IGG-RF-25122000	Limited	*Done (FhG)*	*Built*	Yes	*Done (FhG)*	*Built*	Yes	*Done (FhG)*	*Built*
IGG-ET-04041997	Yes	*Done (FhG)*		Limited					
IGG-EP-26072004	Yes								
IGG-FA-14111998	Yes	*Done (FhG)*		Limited	*Ongoing (FhG)**				
IGG-MM-19102004	Yes			Yes	*Done (FhG)*		Limited		
IGG-ER-11012005	Yes			Yes					
IGG-VA-03112006	Yes			Limited					
OPBG-GC-20082005	Very limited	*Done 1 foot (FhG)*		Very limited	*Ongoing (FhG)**	*Built***	Yes		
OPBG-AA-23012007	Very limited	*Done 1 foot (FhG)*		Yes	*Ongoing (FhG)**				
OPBG-LV-05072001	Yes	*Done (FhG)*	*Built*	Yes	*Done (FhG)*				
OPBG-MG-07012001	Very limited	*Done 1 foot (FhG)*		Very limited			Limited		
OPBG-MT-21082001	Yes	*Done 1 foot (FhG)*		Yes			Limited		
OPBG-FZ-28102007	Yes			Very Limited					
OPBG-SL-16082007	Yes								
OPBG-VF-08092001	Yes			Yes					
OPBG-CR-30042008	Yes			Limited					
OPBG-RD-1611205	Yes								
OPBG-AC-08122005	N/A								

3 Assessment and refinement of the biomechanical modelling workflow presented in D10.1

A workflow to generate patient specific musculoskeletal models of the foot and ankle from relevant MRI images using a supervised atlas registration procedure was presented in deliverable D10.1 and published shortly after (Prinold et al., 2016). These models, joined to a generic musculoskeletal model, were used in biomechanical simulations of gait with the aim of estimating muscles and joint contact forces. The processing pipeline that allowed running those simulations consisted of the following steps:

1) Virtual palpation of anatomical landmarks (i.e. identification of points in a multimodal display interface where bone reconstructions and MRI are visible at the same time (Taddei et al., 2007)) on the bone geometrical models obtained from the MRI images. NMSBuilder was used for this operation (Valente et al., 2014).
2) Registration of a generic atlas of muscle attachments (Arnold et al. (2010) onto the patient specific bone geometries, using an affine transformation defined by the registration of specific bony landmarks (Ascani et al., 2015).
3) Refinement, by manual adjustment based on the MRI images, of the muscle paths obtained by directly connecting the muscle attachments estimated at the previous step.
4) Calculation of the inertial properties of each segment.
5) Creation of the joints connecting the bodies and definition of their axes using selected anatomical landmarks.
6) Fusion of the ankle and foot model to a model of the lower limb. The latter model, according to the available data, can be either a generic scaled model or a patient specific model obtained from month-6 lower limb MRI data.
7) Registration of the markers from the gait lab and the markers visible in the MRI scans in order to associate the gait data to the anatomical model.
8) Simulations of the patient's gait and estimation of the muscle and joint contact forces.

Since this pipeline entails a number of operator-dependent procedures, its critical steps have been tested for repeatability in order to ensure that it can be reliably applied to further cases.

3.1 Assessment of the repeatability of the modelling procedure

The inter- and intra-operator variability in the steps of virtual palpation, manual adjustment of the muscle paths and definition of the joint axes has been investigated as part of this analysis. The robustness of the pipeline was tested involving three operators working on the same three patient datasets (Table 6). Suitable statistical analyses were selected according to the purpose of the investigation.

Table 6: Number of times that a step of the procedure was repeated by each operator on each datasets. The operations were repeated the indicated number of times on all considered three patients. The patients involved in this study were IGG-AP, IGG-JL, OPBG-VL.

	Virtual palpation	Muscle path adjustment	Joint reference systems
Operator 1	3x3x3	3x1x1	3x1x1
Operator 2	3x3x3	1x1x1	1x1x1
Operator 3	3x3x3	1x1x1	1x1x1

3.1.1 Virtual palpation of anatomical landmarks

The generic model was registered on the patient's data using as an atlas the generic lower limb model developed by Arnold et al. (2010). 53 anatomical landmarks were palpated (Figure 5) using a detailed and intuitive atlas of body landmarks available in literature (van Sint Jan, 2007) as visual guide (the complete list of points is available as supplementary material in Prinold et al. (2016)). The anatomical landmarks of interest for the study were virtually palpated by three expert operators, who performed the whole procedure on datasets collected from three patients (IGG-AP, IGG-JL, OPBG-VL). The operators repeated the virtual palpation three times for each dataset in order to assess both inter- and intra- operator reliability.

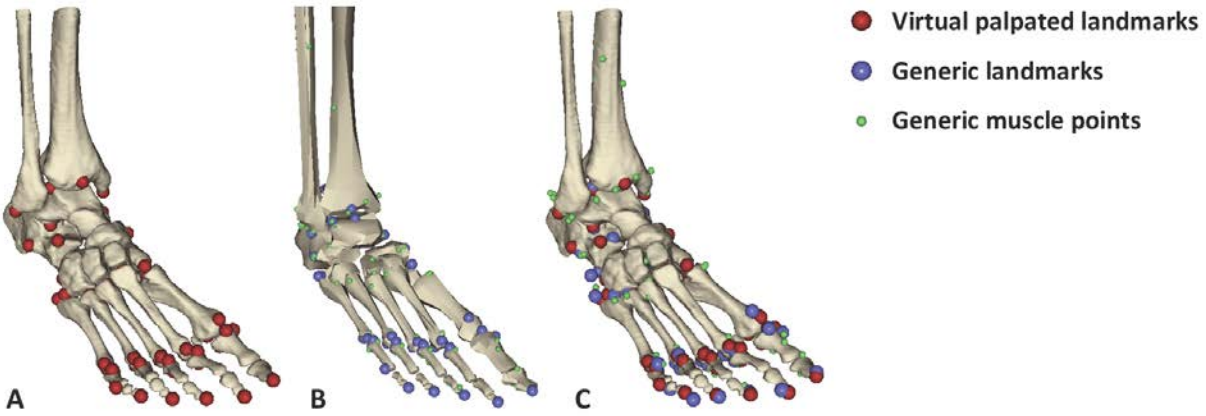

Figure 5: (A) Patient specific foot geometries with virtually palpated bony landmarks (in red) (B) Generic model with virtually palpated bony landmarks (in blue) (C) Registration of points identified in (A) onto the corresponding point identified in (B) and atlas of muscle attachments mapped onto the patient specific geometry (green points).

The coordinates of the points virtually palpated by each operator on three different sessions were collected and processed in order to calculate the palpation's standard deviation across trials for each patient dataset. Standard deviations across evaluators were used to identify the less repeatable markers in the landmark cloud associated with each segment. The markers with the higher standard deviations were deleted from the list of the points to be palpated for that segment after checking that the quality of the registration was not

affected. This check was performed in terms of residuals of the registration and of position of the estimated muscle attachments, using the MRI as a reference. **The reduction of the number of points to the most repeatable subset aimed to enhance consistency among operators and minimize the time required for the palpation.** Once all operators had performed their virtual palpations, the operator-dependent variability was tested by comparing intra- and inter-operator standard deviations between palpated anatomical markers. Each landmark cloud, palpated on the respective body segment (shank, talus, hindfoot, forefoot, toes) was considered independently for a two-tailed paired Student's t-test (level of significance of 0.05). Intra and inter-operators standard deviations across the three trials were computed (Table A.1) and a Student's t-test between the two was performed.

A one-way ANOVA (level of significance of 0.05) was run between the three subjects to test whether differences in standard average errors of palpation were attributable to the anatomy of the patient. One marker, i.e. *tibia_shaft,* required different considerations since its position was bonded in the direction of tibia length and its palpation only involved moving it in plane within the section of the tibia shaft. Although it is included in the statistical analysis, results will be discussed separately.

The markers of the atlas were ranked based on the standard deviation of their location among the trials of palpations. Mean and standard deviations for each patient over 9 trials are available in Table A.2. The mean and standard deviations over the three subjects were also calculated and used to establish a ranking order for the deletion of the markers. Maximum disagreement between operators was observed for *FGA* (sd = 3.98 mm) for Subject 1, *most_inferior* (sd = 4.01 mm) for Subject 2 and *post_inf_cuboid* (sd = 3.11 mm) for Subject 3. All these points were in the hindfoot segment. Mean standard deviations over the three subjects were then calculated. The worst value was reported for the *FGA* marker (sd = 2.84 mm). The progressive deletion of less repeatable markers led to a second, refined Landmark Atlas (A2, see Table 7) including 22 markers.

Table 7: Most repeatable anatomical markers composing the final Landmark Atlas (A2) for Virtual Palpation procedure

Distal shank	
TAM	Distal apex of tibia (by medial malleolus)
FAL	Distal apex of fibula
tib_shaft	centre of the tibia shaft at 20% of ANK to FLE markers
Hindfoot	
FCC	Apex of posterior calcaneous
FPT	Peroneal trochlea (prominence opposite STL)
ant_inf_cuboid	anteriorinferior corner of cuboid (on lateral side)
most_ant	most anterior point on hindfoot (superior too)
Talus	
lat_process	inferior apex of the lateral process
med_tub	apex of the anteriormedial tuberosity
post_proc	most posterior point on the talus
post_med	inferior posteriormedial corner of the talus
Metatarsals	
FMT	Apex of proximal 5th met
FM1	Superior distal head of 1st met
FM5	Superior distal head of 5th met
PMT	Centre of proximal articular 1st met
IDH	Inferior distal head of 1st met
IDM5	Inferior distal head of 5th met
Toes	
D5	Distal point of 5th distal phalanx
DH	Distal point of distal phalanx of hallux
H_s	Superior point on proximal hallux head
H_m	Medial point on proximal hallux head
5_i	Inferior point on proximal 5th phalanx head

Inter- and intra- operator repeatability of virtual palpation was assessed for each patient using a Student's t-test (level of significance of 0.05) comparing standard deviations among different trials. Results of the t-test for the final atlas A2 are reported in Table 8.

Table 8: p values resulting from Student's t-test between intra- and inter-operators standard deviations palpating atlas A2 (22 markers).

Segment	Subject 1 p value	Subject 2 p value	Subject 3 p value
Shank	0.38	0.34	0.88
Talus	0.12	0.45	0.81
Hindfoot	0.32	0.52	0.43
Forefoot	0.78	0.80	0.83
Toes	-	0.82	0.98

The initial landmark atlas (53 markers) was reduced to a subset of 22 markers, which were chosen among the most repeatable (except those indispensable for the successive registration operation). The statistical analysis assessed that no significant differences were remarkable when different operators were performing the virtual palpation, confirming the assumption that no differences in the procedure were imputable to the specific operator. The ANOVA also showed that no significant differences in the standard deviations were due to the specific patient anatomy. Thus **the procedure was operator independent and subject independent.**

One marker, i.e. *tibia_shaft,* required a separate analysis since its position was bonded in the direction of tibia length and its palpation only involved moving it in plane within the section of the tibia shaft. Independently from its repeatability, this marker is fundamental for the successive registration procedure since it is the reference point for the axial alignment of the tibia. Consequently, this marker was identified as **the major cause of axial misalignment between the three models built by the operators.** Even a small angular offset at the ankle joint level could result in a large linear displacement observed at the end of the lower limb chain, i.e. at the pelvis, when the patient specific models were fused to the generic OpenSim model of the lower limb (Figure 6). **As such, a robust procedure to fuse the feet and ankle models from month-0 and month-12 to the months-6 data has been implemented (as detailed in section 4.4) and a significant enhancement of the modelling pipeline has been achieved as a consequence.**

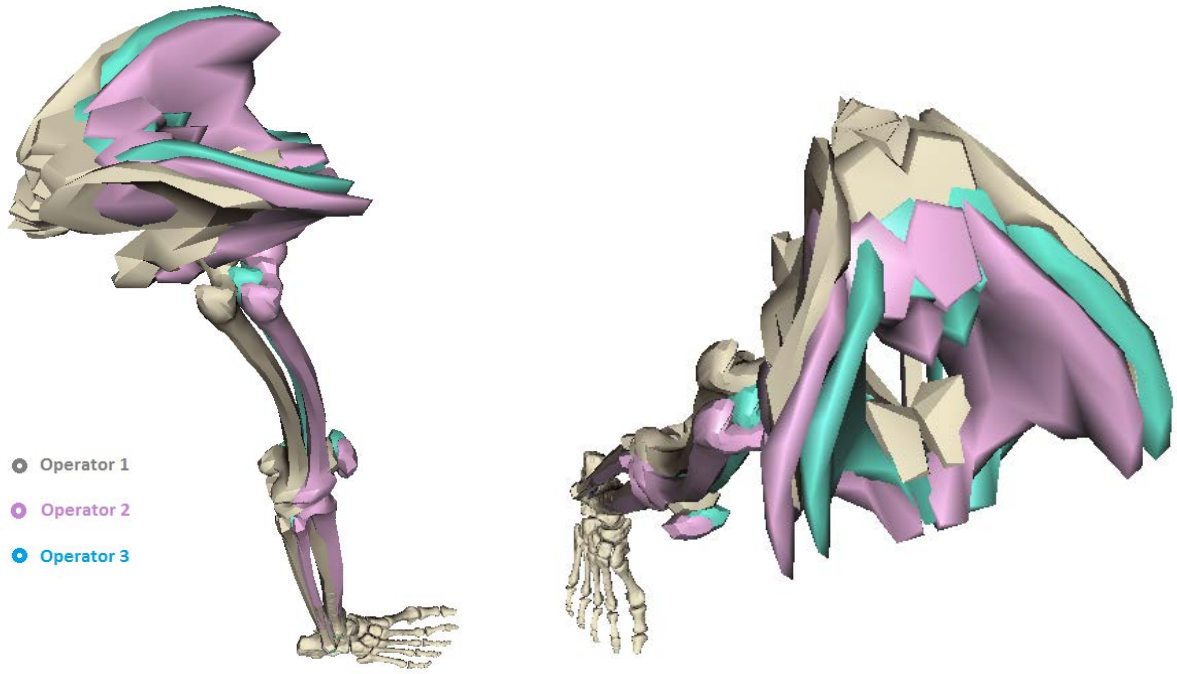

Figure 6: Views of the superimposition of the models built by the three operators. Small linear displacements at the ankle become more evident at pelvis level.

3.1.2 Muscle path adjustment

The muscle attachments were positioned on the patient specific bone geometries by an affine transformation derived from the registration of the bony landmarks. A visual inspection was needed after the registration in order to ensure the correct location of the muscles and that the musculoskeletal model was representative of the individual patient. The inspection is mandatory since the generic model is representative of an adult anatomy whereas paediatric patients may present different anatomical features. In addition, the clinical population involved in the study might present anatomical abnormalities at the foot and ankle, such as joint space narrowing and intra articular bone ankyloses. In order to increase the resemblance to the patient's anatomy, muscles insertions, origins and via points were individually checked and, if necessary, adjusted in NMSBuilder in order to ensure correspondence with the muscle paths in the MRI images (Figure 7). The inter- and intra- subject reliability of this operation was assessed by having three operators repeating it for each patient and one operator repeating it three times for a single patient.

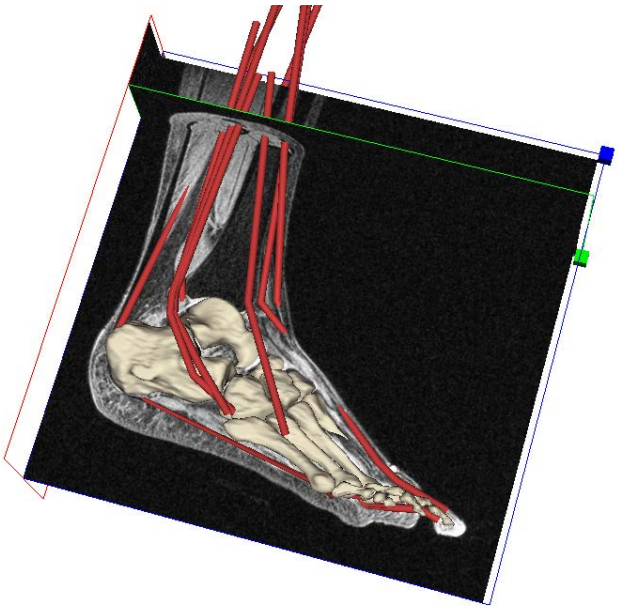

Figure 7: Identification of muscular attachments using the MRI images as reference.

Since one operator repeated the palpation three times for one subject, a statistical analysis between intra- and inter-operators variability was performed for that subject. Standard deviations were calculated for the intra-operator trials and compared to the corresponding standard deviations of the inter-operators trials. For the purpose, a two-tailed paired Student's t-test (level of significance of 0.05) was used.

Mean standard deviations across the subjects were calculated and used to rank muscular attachments according to the variance observed in the palpation. This was useful to understand whether standard deviations of insertions followed a different trend with respect to origins and via point and *vice versa.* Then, the problem was analysed looking at the possibility that peculiarities in anatomical geometries could affect the errors made by the operators while reading the MRI images. A one-way inter-subject ANOVA (level of significance of 0.05) was performed for this purpose. The assumed null hypothesis was that no significant differences in the procedure were attributable to the specific anatomy of the patient considered. To test this hypothesis average standard deviations across operators (within the same subject) were calculated.

Inter- and intra- operator repeatability (Table A.3) in defining muscle paths were assessed for a single patient dataset using a Student's t-test (level of significance of 0.05) to compare standard deviations among trials. Mean standard deviation was 1.77 ± 1.96 mm for the intra-operator trial and 3.00 ± 2.48 mm for the inter-operators trials. The peak intra-operator standard deviation (9.59 mm) corresponded to the *FHB_O* (Flexor Hallucis Brevis origin) attachment. The maximum inter-operators error (14.26 mm) was observed for the *EHB_via* (Extensor Hallucis Brevis via point) attachment. The result of the Student's t-test showed a p value lower than 0.05.

Looking at the variability among the three subjects, standard deviations collected in Table A.4 showed mean values of 2.98 ± 2.91 mm for Subject 1, 3.00 ± 2.48 for Subject 2 and 2.70 ± 2.33 for Subject 3. The least repeatable attachments were *FHB_O* (16.99 mm), *EHB_via* (14.26 mm) and *EDL_via1* (12.30 mm) for the three subjects respectively. The average maximum standard deviation among the subjects was observed at the *FHB_O* attachment (9.03 mm).

The results of the ANOVA showed that no differences were found between the datasets (p=0.66) and hence the null hypothesis had to be accepted that **no differences were due to the specific anatomy of the patients included in the study.**

We found that the procedure of moving muscular attachments (according to MRI images) was highly dependent on the specific operator. In general, the attachments of the toes (i.e. the insertions of Extensors and Flexors Digitorum and Hallucis) were found to be more identifiable in the MRI images, since the operators agreed more in their localization. We reported higher disagreement for via points than for origins and insertions. These results confirm the literature reports that errors in locating muscular attachments are the biggest source of inconsistency of musculoskeletal output (Scheys et al., 2009; Valente et al., 2014; Prinold et al., 2016) and show that a skilled and trained operator is desirable and **call for an automation of this procedure before it can be adopted in larger clinical studies. No differences in the results were found to be attributable to the anatomy of the subject. Still, it is important to stress that in absolute terms the reproducibility error for trained operators is limited to a few millimetres, an excellent result for such a complex modelling protocol.**

3.1.3 Sensitivity of ankle contact forces to variations of muscle attachments

The sensitivity to muscle attachment locations was tested by perturbing each of the points representing the muscles that cross the ankle by 5 mm in the hindfoot coordinate frame. This value was chosen as a reasonable value for human error in virtual palpation of an MRI dataset, given the results reported in Table A.3 and Table A.4. A consistent value across muscle points also allows a comparison of the muscles' relative sensitivities. Only points that were immediately to either side of the ankle joint were used. Perturbations were applied to the Achilles tendon insertion (Figure 8) and the following muscles: Tibialis Anterior, Tibialis Posterior, Peroneus Longus, Peroneus Tertius, Peroneus Brevis, Flexor Hallucis Longus, Flexor Digitorum Longus, Extensor Hallucis Longus, and Extensor Digitorum Longus.

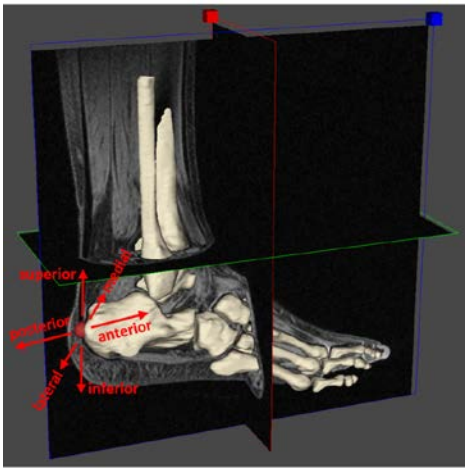

Figure 8: Visual representation of how the insertion of the triceps surae was perturbed in order to assess the sensitivity of ankle contact forces to these changes

As shown in Table 12, model-predicted ankle joint reaction force sensitivity to perturbation of muscle paths appears to be high, indicating the need for a patient specific determination of these points. This is particularly true in the case of the Achilles tendon, where a 5 mm movement in the insertion point leads to a mean change of up to 7.2% and a maximum change of up to 13.4% in the ankle joint reaction force magnitude (Table 9 and Table 10). Ankle joint reaction force also appeared to be sensitive to the Tibialis Posterior muscle via points in all patient models. Some patient models also show some sensitivity to the Peroneous Longus via points and the Tibialis Anterior via points and insertion. The models showed negligible sensitivity to other muscles crossing the ankle, all of which caused mean changes in the ankle joint contact forces of less than 0.5% across stance.

Table 9: Mean percentage change in ankle joint reaction force. Mean values have been computed across the stance phase of gait and across the three trials – original muscle position value subtracted from perturbed muscle position value. Muscles are included that have a mean percentage change of greater than or equal to 0.5% in at least one perturbation in one patient. The colour scale is based on the absolute values and ranges from 7.2 (the maximum value with the highest level of shading) to 0 (with a white background colour). Via points are indicated as "via1, via2, and via3", whereas the insertion points are indicated as "I".

	Achilles	**Peroneus Longus**			**Tibialis Anterior**			**Tibialis Posterior**		
	I	via1	via2	via3	via1	via2	I	via1	via2	I
Patient 1										
Anterior	4.9	0.0	-0.6	0.0	0.0	-0.6	-0.9	-0.2	2.4	0.0
Posterior	-3.5	0.0	0.5	0.0	0.0	0.6	1.1	0.3	-2.0	0.0
Superior	-0.3	0.0	-0.9	-0.1	0.0	-0.7	-0.8	-0.1	-0.7	0.0
Inferior	0.3	0.0	1.2	0.0	0.0	0.9	0.7	0.1	0.6	0.0
Lateral	5.2	0.0	-0.9	-0.2	0.0	-1.1	-1.8	0.3	4.1	0.0
Medial	-4.4	0.0	0.9	0.2	0.0	1.2	2.4	-0.2	-2.7	0.0
Patient 2										
Anterior	5.3	-0.1	-0.2	0.0	-0.1	-0.5	-0.6	-0.2	2.3	-0.1
Posterior	-4.5	-0.1	0.0	-0.1	-0.1	0.3	0.6	0.1	-2.1	-0.1
Superior	-0.6	-0.1	-0.2	0.0	-0.1	-0.3	-0.1	0.0	1.1	-0.1
Inferior	0.5	-0.1	0.1	-0.1	-0.1	0.3	0.0	0.1	-0.8	-0.1
Lateral	5.3	-0.1	-0.4	0.0	-0.1	-1.1	-1.3	1.6	2.7	-0.1
Medial	-4.3	-0.1	0.4	-0.1	-0.1	1.1	1.3	-1.3	-2.1	-0.1
Patient 3										
Anterior	7.2	-0.2	-0.2	-0.2	-0.2	-0.4	-0.4	-0.3	4.8	-0.2
Posterior	-5.8	-0.2	-0.2	-0.2	-0.2	0.1	0.1	0.1	-4.2	-0.2
Superior	-0.4	-0.2	-0.2	-0.2	-0.2	-0.4	-0.3	-0.2	-1.1	-0.2
Inferior	0.1	-0.2	-0.2	-0.2	-0.2	0.1	0.0	0.0	0.5	-0.2
Lateral	-5.4	-0.2	-0.2	-0.2	-0.2	-0.2	-0.1	-0.4	-3.7	-0.2
Medial	5.3	-0.2	-0.2	-0.2	-0.2	0.2	-0.1	0.4	5.1	-0.2

Table 10: Maximum value of percentage change in ankle joint reaction force. Values (mean over three gait trials) have been calculated in the stance phase of gait – original muscle position value subtracted from perturbed muscle position value. Muscles are included that have a mean percentage change of greater than or equal to 0.5% in at least one perturbation in one patient. The colour scale is based on the absolute values and ranges from 13.4 (the maximum value with the highest level of shading) to 0 (with a white background colour). Via points are indicated as "via1, via2, and via3", whereas the insertion points are indicated as "I".

	Achilles	**Peroneus Longus**			**Tibialis Anterior**			**Tibialis Posterior**		
	I	via1	via2	via3	via1	via2	I	via1	via2	I
Patient 1										
Anterior	10.6	-0.6	-2.8	-0.6	-0.6	-3.0	-2.9	-1.3	5.2	-0.6
Posterior	-8.2	-0.6	2.5	-2.2	-0.6	3.0	3.3	0.7	-4.3	-0.6
Superior	-1.7	-0.6	-3.8	-0.6	-0.6	-3.1	-2.4	-1.0	-1.5	-0.6
Inferior	1.4	-0.6	5.3	-2.0	-0.6	4.1	2.2	-0.6	1.5	-0.6
Lateral	13.4	-0.6	-3.4	-0.9	-0.6	-3.8	-5.5	1.0	8.2	-0.6
Medial	-12.0	-0.6	3.8	0.8	-0.6	3.9	5.8	-1.0	-5.4	-0.6
Patient 2										
Anterior	9.6	1.2	-2.0	1.3	1.2	-2.7	-2.8	-1.0	4.4	1.2
Posterior	-7.9	1.2	1.5	-1.2	1.2	2.4	2.2	2.0	-3.8	1.2
Superior	-1.5	1.2	-2.5	1.3	1.2	-2.5	-1.5	-1.0	2.1	1.2
Inferior	1.6	1.2	2.6	1.1	1.2	2.4	1.5	2.0	-1.5	1.2
Lateral	11.5	1.2	-3.5	1.3	1.2	-4.5	-4.6	2.8	4.8	1.2
Medial	-11.9	1.2	3.8	1.1	1.2	3.8	3.9	-2.1	-3.5	1.2
Patient 3										
Anterior	12.9	-0.8	-1.0	-0.8	-0.8	3.2	-2.3	-0.9	7.8	-0.8
Posterior	-9.9	-0.8	-0.9	-0.8	-0.8	-3.0	2.4	0.6	-6.5	-0.8
Superior	2.0	-0.8	-2.6	-0.8	-0.8	-2.6	-1.6	-0.9	-1.6	-0.8
Inferior	-2.4	-0.8	-2.4	-0.8	-0.8	-3.1	-1.0	-0.6	0.9	-0.8
Lateral	-9.3	-0.8	-1.3	-0.8	-0.8	-3.4	3.3	-1.0	-5.0	-0.8
Medial	9.4	-0.8	-2.3	-0.8	-0.8	3.8	2.0	0.9	6.7	-0.8

3.1.4 Joint axes definition

The palpation of the appropriate points used to define segmental frames is another operator dependent procedure. To identify the origins and orientations of the frames, the operators palpated appropriate bony landmarks on the patient specific geometry. Anatomical coordinate frames were defined for the shank, hindfoot, forefoot, and toes using NMSBuilder (Figure 9). The coordinate systems were defined after the partially modified Stebbins et al. Oxford Foot Model (2006) by identifying meaningful virtual palpated landmarks or gait markers as reference. Each operator performed the palpation independently and one operator performed it three times.

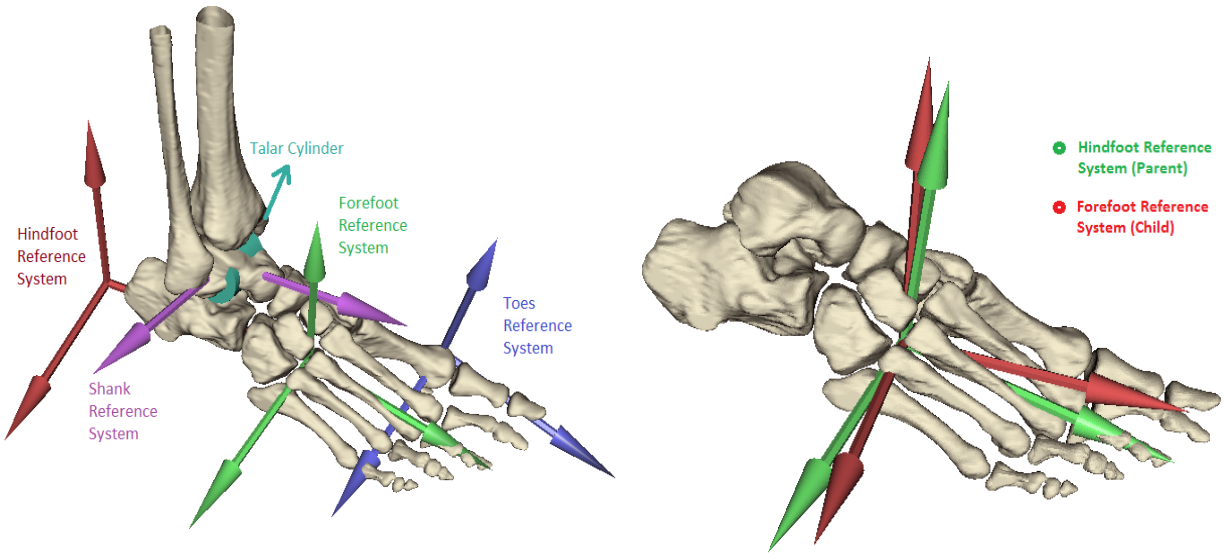

Figure 9: Segmental frames palpated on the foot segments (left). Definition of foot joint by means of two segmental frames: the parent (proximal) and the child (distal) sharing the same origin (i.e. the joint center) (right).

The angles between proximal and distal segments of each joint of the foot were calculated using the rotations that superimpose the proximal frame to the distal frame if a cardan rotation is applied and the values found across operators were compared within each subject. Table 11 shows the inter-operator differences in defining articular frames for each of the subjects and operators. The initial configuration of the kinematic chain depends on the defined joint reference systems and their positions and orientations, so offsets between the models built by the operators might be introduced. The rotations (in degrees) around each axis of the distal frame to reach the configuration of the proximal frame were chosen to compare the models built by different operators (Figure 10). For each subject mean values and standard deviations between operators were also calculated.

Table 11: Measured inter-segmental angles at each foot joint in the MRI position where they were defined: hindfoot/tibia (HF/TB), forefoot/hindfoot (FF/HF), toes/forefoot (TO/FF). Angles are measured about antero-posterior (x), inferior-superior (y), medio-lateral (z) axes.

	Subject 1								
Joint	**Operator 1**			**Operator 2**			**Operator 3**		
	x (deg)	**y (deg)**	**z (deg)**	**x (deg)**	**y (deg)**	**z (deg)**	**x (deg)**	**y (deg)**	**z (deg)**
HF/TB	-9.77	-19.55	-25.28	-7.06	-14.93	-22.25	-8.41	-21.68	-24.84
FF/HF	0.62	-2.76	-3.97	-6.25	1.53	-6.65	-4.38	4.81	-9.29
TO/FF	0.00	0.00	8.79	0.00	0.00	7.67	0.00	0.00	12.28
	Subject 2								
	Operator 1			**Operator 2**			**Operator 3**		
	x (deg)	**y (deg)**	**z (deg)**	**x (deg)**	**y (deg)**	**z (deg)**	**x (deg)**	**y (deg)**	**z (deg)**
HF/TB	14.70	-1.00	-9.84	14.73	4.82	-9.39	12.36	9.67	-9.83
FF/HF	6.78	-14.30	-5.58	4.50	-8.09	-3.83	5.73	-7.93	-5.05
TO/FF	0.00	0.00	-3.90	0.00	0.00	-9.35	0.00	0.00	-10.06
	Subject 3								
	Operator 1			**Operator 2**			**Operator 3**		
	x (deg)	**y (deg)**	**z (deg)**	**x (deg)**	**y (deg)**	**z (deg)**	**x (deg)**	**y (deg)**	**z (deg)**
HF/TB	-11.57	-1.99	-14.63	-7.01	-8.62	-16.41	-5.86	-5.59	-18.06
FF/HF	-4.05	10.11	-2.62	-8.05	11.64	-3.32	-8.10	9.37	-11.61
TO/FF	0.00	0.00	-8.14	0.00	0.00	-5.52	0.00	0.00	5.15

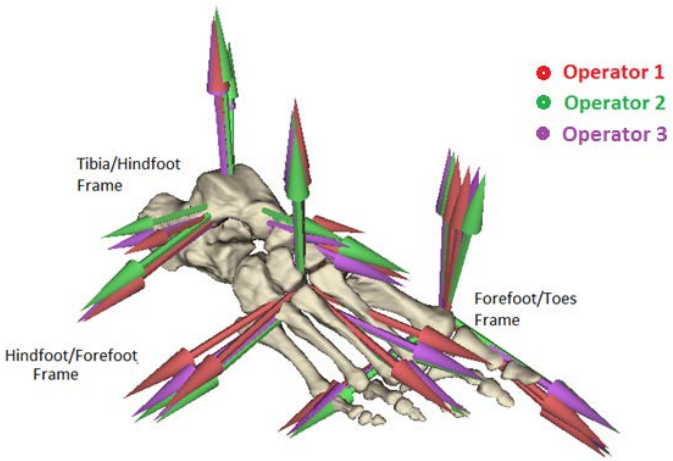

Figure 10: The segmental frames involved in the three intrinsic joints of the foot. Each joint is defined by a parent frame (on proximal segment) and a child frame (on distal segment). Three colours (representing the three operators) are used to stress the variations due to the operator-dependence of the procedure

Inter-operator variability was evaluated in terms of standard deviations of the foot joint angles as derived from the manual joint definition. Inter-segmental angles were measured in the antero-posterior direction (x), inferior-superior direction (y) and medio-lateral direction (z). Table 12 shows the mean values for the

above described angles for each foot joint considered. The respective standard deviations varied between 0.26 deg and 7.04 deg.

Table 12: Means across the evaluators of the inter-segment angles between parent and child reference systems. Hindfoot/tibia (HF/TB), forefoot/hindfoot (FF/HF), toes/forefoot (TO/FF).

	Subject 1			Subject 2			Subject 3		
	mean (deg)			mean (deg)			mean (deg)		
Joint	**x (sd)**	**y (sd)**	**z (sd)**	**x (sd)**	**y (sd)**	**z (sd)**	**x (sd)**	**y (sd)**	**z (sd)**
HF/TB	-8.41 (1.36)	-18.72 (3.45)	-24.12 (1.64)	13.93 (1.36)	4.50 (5.34)	-9.69 (0.26)	-8.15 (3.02)	-5.40 (3.32)	-16.37 (1.72)
FF/HF	-3.34 (3.55)	1.19 (3.80)	-6.64 (2.66)	5.67 (1.14)	-10.11 (3.63)	-4.82 (0.90)	-6.73 (2.32)	10.37 (1.16)	-5.85 (5.00)
TO/FF	0.00	0.00	9.58 (2.40)	0.00	0.00	-7.77 (3.37)	0.00	0.00	-2.84 (7.04)

Some operator-dependent variability in the orientation of adjacent segments was found, even if this aspect was less dramatic than the others investigated within the study. **The issue of the repeatability of joint axes definition could be solved by introducing semi-automatic fitting routines. These have now been implemented and will be described in the section dedicated to the updated modelling pipeline.**

3.1.5 Summary of findings

The study described in this section of D10.4 was designed to investigate the repeatability of three critical steps of the modelling pipeline used to generate patient specific models of the foot and ankle joint; virtual palpation of bony landmarks, manual adjustment of muscle paths and the definition of foot joint axes.

The virtual palpation was found to be a repeatable operation, both intra- and inter-operator, and allowed for a refined subset of bony landmarks to be determined from the generic atlas initially developed. As a result of the study, **the 22 most repeatable bony landmarks were identified and used to define a new atlas** that will be adopted for processing future patients.

The manual adjustment of muscle attachments, even if performed by experienced operators using multiple MRI sequences, has been shown to be a highly operator-dependant step of the current pipeline. These results affect the biomarkers that will be extracted using the biomechanical model in the measure that the lack of repeatability affects ankle contact forces. Assessing the sensitivity of the articular loading at the tibio-talar joint to perturbation of the muscle attachments it was found that **misplacement of the path of muscles with larger physiological cross sectional area and moment arm, i.e. *triceps surae*, *tibialis anterior*, *tibialis posterior* and *peroneus longus*, can affect contact forces. Therefore, special care has to be devoted when locating their bone insertions.** Still, even in the worst case scenarios, the sensitivity to overestimated uncertainty in the anatomical modelling was never much larger than 10%. And most of these errors were related to the Achilles' tendon, that from now on will be individualised with particular care, as we are aware

of the model's sensitivity to this particular input; thus, it is realistic to expect that in most cases sensitivity to anatomical uncertainty will never exceed 2-3%. Considering that subject-specific models of this complexity in any case produce predictions that are never more accurate than 90%, this level of sensitivity seems perfectly acceptable for the purpose.

Finally, the identification of joint axes appeared to be less critical than the other two steps, although the **introduction of semi-automatic tools in joint definition** would represent a further improvement.

The findings of this repeatability study, and previous work based on this modelling pipeline (Prinold et al., 2016), lead to the conclusion that models should be personalised as much as possible. When this is not fully achievable due to technical difficulties, e.g. in muscle paths definition, efforts should still be made to personalise the critical geometrical elements of the model at least.

4 Refinement of the biomechanical modelling workflow

As a consequence of the results of the repeatability study and of the application of the original pipeline to a larger number of patient datasets, a series of improvements have been introduced to address the following shortcomings that emerged when using the previous workflow:

1. *Generation of the generic model*: The fusion between patient specific ankle models (month 0-12) and the generic model was originally performed in NMSBuilder (NMSB), the same software environment used for the virtual palpation and muscle paths definition. Despite technically correct, this choice turned out to be extremely time-consuming for the following reasons:
    a. The generic model of Arnold et al. had to be scaled in the NMSBuilder software environment, with each segment being resized using scale factors calculated separately, according to lengths estimated from the gait analysis markers.
    b. Once the generic model has been scaled and the patient specific ankle has been fused (by registering bony landmarks virtually palpated on the two tibias), an OpenSim model can be generated from NMSB. However, the lower limb model of Arnold et al. includes 17 wrapping surfaces, used to describe the muscle paths around the bones, which cannot be exported from NMSBuilder. This forces the operator to manually include them in the OpenSim model.
    c. The model of Arnold et al. (2010) includes both a knee and a patellofemoral joint, which cannot be defined directly in NMSBuilder. A manual modification of the OpenSim file is required for this purpose.
2. *Generation of the patient specific ankle and foot model*: The original pipeline did not include a procedure to correct for possible inversion/eversion offsets that might result from an incorrect patient position (i.e. non parallel feet) during the MRI scan. Since no subtalar joint was modelled, the relative position of tibia and calcaneus could not be modified in order to match the standing

reference position of the foot (Figure 11). This limitation in the degrees of freedom of the model can lead to large errors in the registration of the gait markers onto the patient specific model, as shown in Figure 11.

3. *Generation of the lower limb patient specific model:*
    a. The procedures for the estimation of critical patient specific musculotendinous parameters such as optimal fibre length and tendon slack length needed to be specified.
    b. The method for fusing the month-0 and month-12 models into the month-6 lower limb model described in D10.1 was the same as fusing the generic model to the patient specific ankles. That procedure, based on rigid registration of palpated landmarks, did not take advantage of the patient specific geometry available in both models.

In addition to the above limitations of the original pipeline, the following objectives have also been achieved:

1. reducing the overall processing time needed to produce a model by minimizing the number of manual operations performed;
2. achieving maximum modularity in producing models of different levels of personalisation (generic scaled models, scaled models with patient specific feet and ankles, fully patient specific models), which would allow incomplete datasets to be better dealt with.

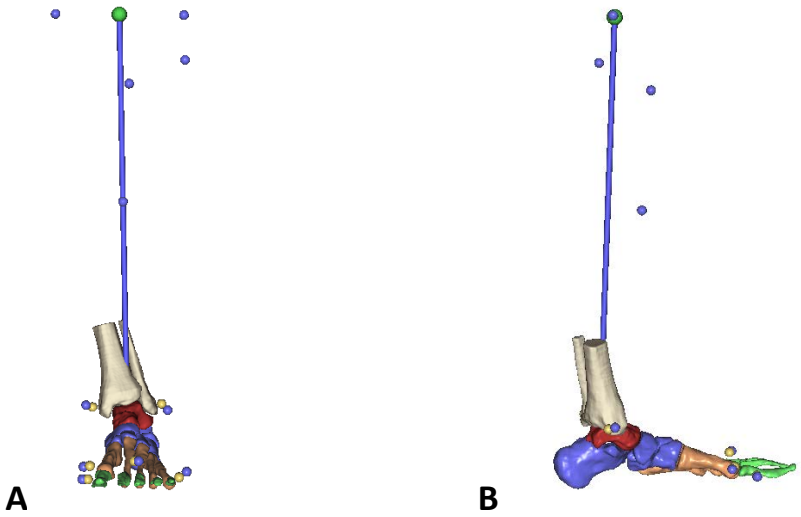

Figure 11: Frontal (A) and side (B) view of the offsets introduced by the previous model definition when registering gait markers on the MRI models without correcting for subtalar joint movement. The yellow markers were available from the MRI scans, the blue markers are from a standing reference trial collected in the gait lab. The blue line represents the longitudinal axis of the tibia estimated from gait lab markers, the green marker being the knee joint centre.

4.1 Generation of the generic model

The model based on Delp et al. (1990) (called 'gait2392' in the OpenSim distribution) has been preferred to Arnold et al. (2010) as a generic atlas for registration into the patient specific geometries. The advantages of this model over the model of Arnold et al. (2010) for the specific aims of this project are several. Firstly, the

model of Delp et al. (1990) does not include wrapping surfaces. Considering that: 1) the wrapping surfaces in the model Arnold et al. (2010) were dimensioned in order to match muscle moment arms from the literature and might not scale linearly with segment dimensions and 2) they cannot be adapted to the month-6 geometries without assumptions in terms of their position and orientation, it seem a reasonable and practical modelling choice to prefer a simpler but more flexible muscle path definition. Secondly, gait2392 does not include an explicit patella-femoral joint, which is instead modelled using via-points that become active after a certain degree of knee flexion. This feature largely simplifies the modelling procedure without loss in model complexity for the specific aims of this project. Thirdly, the characteristics of muscle attachments and muscle paths of gait2392 are very similar to those of the previous model, both in terms of number of muscle attachment points and their spatial collocation, i.e. the differences are mainly in the muscle contraction parameters, which for patient specific models are not available in any case and in our models will be estimated using an optimization procedure described in section 4.3.2. **In summary, it has been considered safe to transition from a generic model based on Arnold et al. (2010) to that of Delp et al. (1990) for the supervised atlas registration performed in this project.**

The generic scaled models to be fused with patient specific ankle models are now obtained through use of the scaling tool available in OpenSim (Delp et al., 2007) instead of using NMSBuilder. This OpenSim tool allows scaling of the lower limb segments by automatically applying scale factors calculated from the ratio between the distances of corresponding marker pairs. The first marker pair is taken from the experimental acquisition, the second is the corresponding virtual marker pair included in the model. An advantage of this procedure is that it entirely decouples the generation of the patient specific model from the fusion of the patient specific ankle models, so it is not necessary to execute this operation in the NMSBuilder software environment. In addition, once the appropriate setup files are produced, the scaling operation only takes a few minutes because it is not necessary to scale each element of the model separately (bones, muscle attachments, etc.).

4.2 Generation of the patient specific foot and ankle model based on the 0 and 12 months MRI data

The procedure described in D10.1 to create patient specific foot and ankle models has been revised and enhanced. The foot model was modified by replacing the joint between hindfoot and midfoot with a subtalar joint. This led to a different definition of the foot segments; the hindfoot and midfoot of the previous model were replaced by a talar segment and a segment (called ‘calcn’) consisting of both the calcaneus and midfoot.

4.2.1 Alignment of the joints

The kinematic model of the foot in the updated procedure can be built based on three virtually palpated landmarks on the lowest point of the calcaneus (called "*most_inferior*" in the atlas) and 1st and 5th metatarsal heads ("IDM" and "IDM5"). These three points are used to identify the frontal pointing axis on the sole of the foot, defined by the vector pointing from "*most_inferior*" to the midpoint of "IDM" and "IDM5", which is used, together with the ankle axis of rotation, to align the reference systems of the metatarsophalangeal and tibiotalar joints. Even though the first of these three points was found to be not repeatable, it has only a minor impact on the kinematic model construction. For instance, for the patient considered in section 5, a 4 mm variation of the "*most_inferior*" calcaneus point would lead to a variation of about 3° in the frontal axis orientation, suggesting an acceptable robustness with respect to the variability of the virtually palpated landmarks.

4.2.2 Talocrural joint axis definition

A cylinder was fitted to the talar trochlea with the talocrural axis of plantar/dorsi-flexion defined as the axis of this analytical surface. In order to improve repeatability and minimize operator intervention, the cylinder is fitted following this procedure: 1) the operator selects the articular surface using Meshlab 2) a cylinder is fitted in a least squares sense (Figure 12 A) using the LSGE Matlab library (http://www.eurometros.org) yielding the parameters of the analytical surface. This freeware library was assessed and verified against *ad hoc* generated test cases before its inclusion in the modelling pipeline.

4.2.3 Subtalar joint definition

The definition of the hind-foot segment described in D10.1 and in Prinold et al. (2016) has the shortcoming of not correcting misalignment due to erroneous foot position in the MRI scan, which might introduce errors in the registration of the gait markers. In order to allow for adjustment of the relative position of the calcaneus, mid-foot (and attached markers) and talus, a subtalar joint was defined as in Parr et al. (2012). A sphere was fitted to the talo-calcaneal joint surface (selected on the talar bone using Meshlab) and a second sphere was fitted to the talo-navicular articular surface (selected on the surface of the navicular bone). The two spheres (see Figure 12 B) were identified using a least squares fitting script implemented in Matlab. The axis of the subtalar joint was defined as the line passing through the centres of the two spheres (Parr et al., 2012).

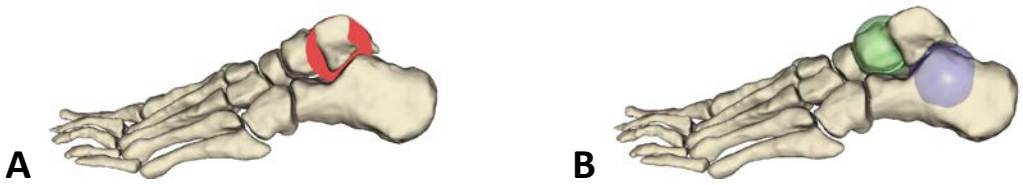

Figure 12: (A) Cylinder fitted in a least squares sense to the talar trochlea (B) Spheres fitted to the talo-navicular articular surface (in green) and to the talo-calcaneal articular surface (in purple) in order to define the subtalar joint axis as a line between the spheres centres

4.2.4 Toes joint definition

Although a single segment foot will be used for these simulations, the toes (phalanges) were still modelled as a separated segment, connected to the midfoot via a hinge joint whose axis was defined similarly to Delp et al. (1990), i.e. joining the centres of 1st and 5th metatarsophalangeal joints. This choice is motivated by maintaining consistency with the model of Delp et al. (1990) and allowing the possibility of future analyses employing multi-segment foot models.

4.3 Generation of the patient specific lower limb model based on the 6-month MRI data

The procedure for generating a patient specific model of the lower limb was described in D10.1, and applies to the entire lower limb the same procedural steps summarised in section 3 of this Deliverable. Two aspects of the procedure not included in the previous document are detailed here, i.e. the computation of the inertial parameters and the optimisation of the muscle parameters.

4.3.1 Computation of segment inertial properties

The geometrical models produced by FhG from the MRI images include bone and skin meshes. The identification of the various body segments has been obtained through planes of section following previous literature on the topic (Zatsiorsky and Seluyanov, 1983; de Leva, 1996). A first section plane, inclined by ~45° with respect to the transversal plane and passing through the hip joint centre, divides the pelvis and thigh. A second plane separates the thigh and the shank with a cut parallel to the transverse plane at the lateral femoral epicondyle. Finally, a transversal section plane at the height of the lateral malleolus identifies shank and foot. Using Netfabb (http://www.netfabb.com), the described cutting planes (summarised in Figure 13 A) were used to section the mesh of the external skin and produce the individual body segments, whose inertial properties (position of centre of mass, mass, tensor of inertia) were finally calculated in NMSBuilder. Different densities were assigned to bone (1.42 g/cm^3) and soft tissue (1.03 g/cm^3 for males and 1.02 g/cm^3 for females), using the values reported in Dumas et al. (2005). A negative soft tissue density was assigned to

any bone volume intersecting the soft tissue volume (Figure 13 B), so that the bone volume (including that of pelvis) was not considered both as bone and soft tissue.

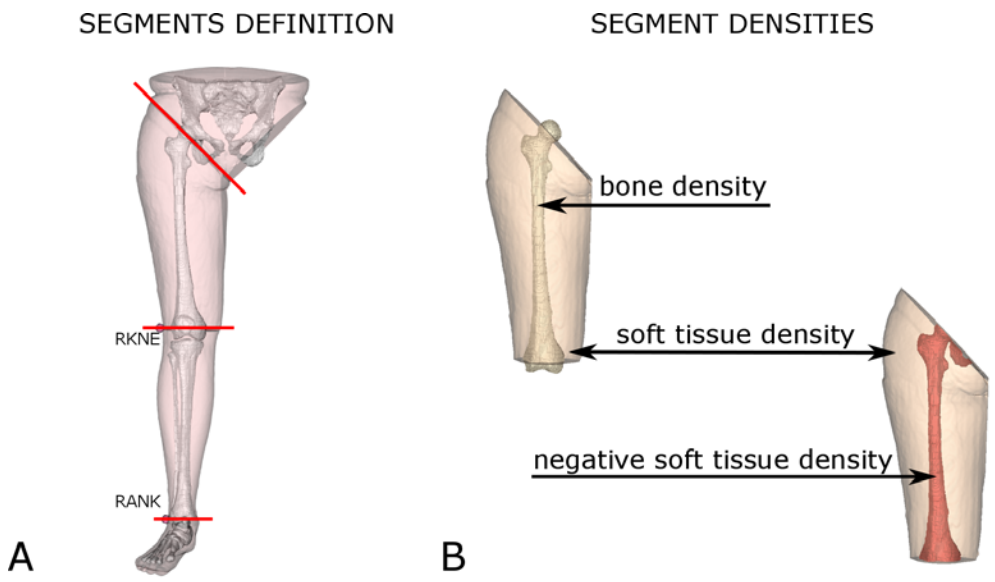

Figure 13: (A) frontal view of the section planes used to define the body segments in the musculoskeletal models (B) description of the different densities assigned to the element of each bones (bone, soft tissue and negative soft tissue).

4.3.2 Optimisation of muscle parameters

Phenomenological Hill-type muscle models are commonly used in biomechanics simulations (Hill, 1938; Zajac, 1989; Thelen, 2003), where the contractile behaviour is modelled without consideration of the mechanistic causes of the force generation. The adopted muscle model includes three elements (Figure 14 A):

1. a contractile element (CE) producing force as a function of its length (force-length relationship (Gordon et al., 1966), Figure 14 A) and contraction velocity (force-velocity relationship (Hill, 1938)). In isometric conditions, a muscle is assumed to generate a maximum isometric force F_{iso}^{m} when its fibre length equals a certain optimal fibre length l_o^m, representing the optimal overlap of thin and thick filaments in the sarcomers composing the muscle fibres. In isokinetic conditions, the muscle force decreases with increasing speed of contraction until a maximum contraction velocity v_{max}^{m} (generally assumed to be 10 l_o^m/s) for which the generated force is zero.
2. a passive elastic element in parallel (PE), accounting for the elastic force produced by the muscle when stretched over l_o^m (Figure 14 B, dashed line).
3. a passive elastic element in series (SE) that represents the tendon. This element, after an initial non-linear toe region, behaves as a linear elastic spring generating force proportional to the displacement from a tendon slack length l_s^t.

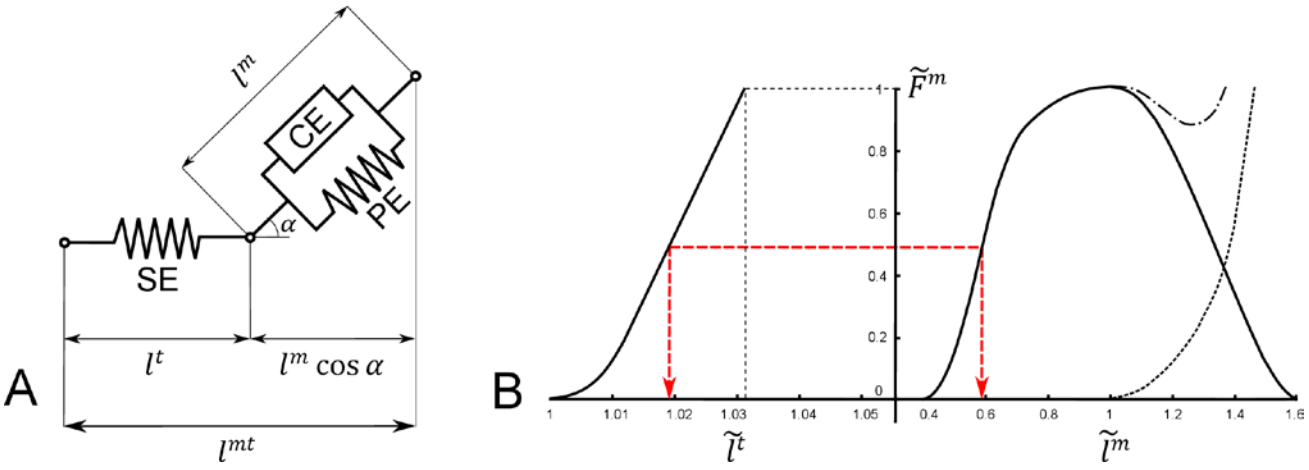

Figure 14: (A) representation of the Hill-type muscle model used in this simulations including a contractile element (CE) connected to an elastic element in series (SE) and one in parallel (PE). (B) Generic curves defining the dimensionless material properties of the tendon (left side, dashed line identifying $\tilde{l}^t = 1.033$ for which $\tilde{F}^m$=1) and muscle (right side, solid line: active force, dashed line: passive force, dash-dot line: total muscle force). In this plots, values on axes are defined as follows (Zajac, 1989) $\tilde{l}^m = l^m/l_o^m$, $\tilde{l}^t = l^t/l_s^t$ and $\tilde{F}_{iso}^m = F^m/F_{iso}^m$, where the apex "m" indicated muscle related quantity and "t" a tendon related quantity. An equilibrated isometric contraction of a muscle with fibers aligned with the tendon (zero pennation angle) is also represented (red dashed line and arrows pointing to the correspondent normalized tendon and fiber length). Figure adapted from from Modenese et al. (2016).

In OpenSim, muscle models are dimensionless (Zajac, 1989), in the sense that force-length, force-velocity and tendon force-strain relationships are normalized using the values of l_o^m, l_s^t, v_{max}^m and F_{iso}^m, obtaining curves like those represented in Figure 14 B. In order to define a muscle, five parameters are needed; optimal fibre length l_o^m, tendon slack length l_s^t, pennation angle at optimal fibre length, maximum isometric force F_{iso}^m and maximum contractile velocity. It has been shown in the literature that muscle force estimation is critically dependent on the values of optimal fibre length l_o^m, tendon slack length l_s^t and maximum isometric force (Scovil and Ronsky, 2006; Redl et al., 2007; De Groote et al., 2010), however, while maximum isometric force is proportional to muscle volume (Ward et al., 2009) and could be estimated by segmenting individual muscles in the MRI images, the other two contractile parameters cannot be estimated from medical images and data routinely collected in the gait lab. Pennation angle at optimal fibre length is generally taken from the literature with v_{max}^m, as anticipated above, assumed to be 10 l_o^m/s.

In the literature methods relying on functional (Garner and Pandy, 2003; Lloyd and Besier, 2003) or anthropometric (Manal and Buchanan, 2004; Hainisch et al., 2012) measurements have been proposed to estimate these parameters. In the patient specific models presented here, we estimated l_o^m and l_s^t by applying the anthropometric methods proposed by Modenese et al. (2016). The method, which is a generalization of Winby et al. (2008), involves preserving the contractile conditions of muscle fibres and tendons (normalized against l_o^m and l_s^t respectively) from a reference model (in this case gait2392) in the subject specific model. This principle is applied to a set of joint angle configurations, common between the two models. The method assumes the same operating range in the force-length curve for the same muscle in different individuals, and has been previously assessed against cadaveric data yielding consistent results with the measurements of Ward et al. (2009). Considering that juvenile idiopathic arthritis does not directly affect

muscles, this assumption can be safely considered valid. The conceptual workflow of the applied method is represented in Figure 15, adapted from Modenese et al. (2016).

Muscle maximum isometric forces F_{iso}^{m} were estimated using a scaling based on body mass, i.e. the maximum isometric force was scaled using the ratio between the mass of the patient and the mass of the generic model. This simple procedure has several limitations: 1) it assumes that maximum isometric forces are proportional between adults and children 2) it assumes that the disease is not affecting muscle volume distribution (which might not be true for paediatric populations) 3) it cannot correct for differences in body mass composition between a child and a generic model, e.g. it does not take into account the percentage of fat mass.

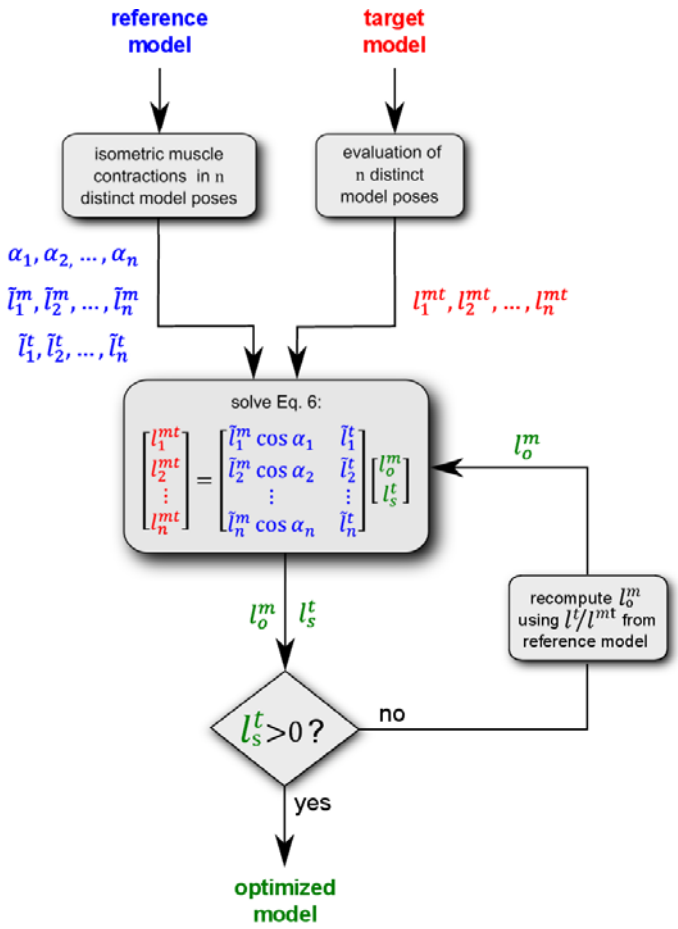

Figure 15: Workflow of the optimisation method used to estimate optimal fibre lengths and tendon slack lengths in the entire patient specific lower limb models. Musculotendon parameters produced as output by the blocks are coloured according to the model they are related to (blue: reference model, red: target model, green: optimized model). (Adapted from Modenese et al. (2016)).

4.4 Combination of the models obtained at the different time points

As anticipated above, after producing patient specific models of the ankle and foot (month-0 and month-12) and of the full lower limb (month-6), a critical step of the modelling pipeline is to either fuse these models or to attach the foot models to a scaled generic lower limb model. This procedure has now been made more robust according to the results of the repeatability study (Figure 11).

The iterative closest point algorithm (ICP) (Besl and McKay, 1992) is used to register the patient specific partial bone geometries from month-0 and month-12 data to the month-6 data. ICP is a registration algorithm that searches for a transformation that minimizes the distance (mean squared error) between a target point cloud (month-6 geometry) and a source point cloud (month-0 or month-12 geometry). The registration was performed in Meshlab and yielded a transformation (rotation matrix plus translation vector) that was used directly in the OpenSim model to fuse the month-6 model with the patient specific ankle models from the other time points.

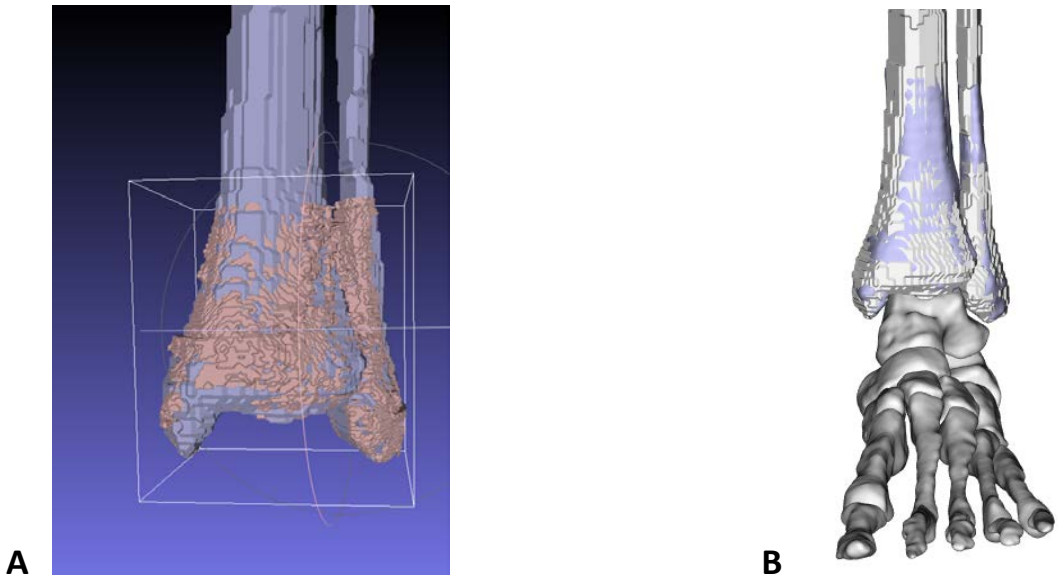

Figure 16: (A) Example of registration of month-12 bone geometries (pink partial tibia and fibular) into month-6 data (light purple full tibia and fibular) using ICP (Besl and McKay, 1992) and (B) foot and ankle model fused in the lower limb model in OpenSim using the transformation calculated by ICP.

4.5 Registration between the anatomical model and gait data

In order to calculate joint angles from the measurement of marker trajectories using the inverse kinematics technique (Lu and O'Connor, 1999) it is necessary to include virtual markers in the musculoskeletal model of the lower limb. These virtual markers are defined by their location with respect to the segment they are attached to, and a calibration step is performed to position them as accurately as possible with respect to the experimentally measured positions.

The marker registration uses a static trial recorded in the gait lab and is performed in three different ways depending on whether; 1) the lower limb model is a generic scaled model, 2) the musculoskeletal lower limb model is derived from month-6 data, in which case the skin markers are visible in the MRI scans and 3) a patient specific model of the lower limb is available from month-6, but the time point of interest is month-0 or month-12, when the patient anthropometry might be different due to natural growth of the subject.

If the lower limb model is a generic scaled model, the virtual markers used in the simulations are those placed in the generic model using the geometries provided with the OpenSim model as a reference. These are adjusted automatically by the marker placer tool after the scaling.

Month-6 patient specific models of the lower limb can incorporate markers in the position observed in the MRI scans. These positions are derived from a scan with the subject laying supine, so the same marker placer tool described for generic models is applied also in this case, although the changes in virtual markers locations are usually small (<1 cm).

When the month-6 lower limb model is used for month-0 and month-12 simulations, the model is scaled linearly using estimated segment lengths from gait analysis measurements. The mass will be also scaled to match the mass of the patient at that time point, maintaining the mass proportions calculated at month-6.

In all cases, the marker adjustment can be evaluated a posteriori through the marker tracking errors reported throughout the inverse kinematics simulations, which ideally should be lower than 2-4 cm with a root mean squared error smaller than 2 cm[1].

4.6 Calibration of knee joint angles offsets

When building the month-6 model, the knee joint was initially treated as a ball and socket joint. Inverse kinematic tracking only anatomical markers in the standing reference position allowed the lower limb model to be positioned as close as possible to the experimental pose. In this pose the non-sagittal joint angles were locked to their current value with the medio-lateral axis used as the flexion-extension knee joint axis. A similar procedure was used to define the metatarsophalangeal and subtalar joint angle offsets in the standing trial before locking them.

5 Walking simulations

At the time of writing, the data available allowed the entire pipeline described above to be implemented for one patient, who underwent 0, 6 and 12 months examinations; the team has now started to model all data available. The following paragraphs describe the relevant procedures and results, with the aim of providing an example of how future data will be used and analysed in spite of the clinical questions coming from WP5.

The MRI scans and geometrical bone reconstructions available for patient IGG-RF (female, 13 years old at month-0) were used to generate models for month-0 (2 ankle models), month-6 (bilateral lower limb model) and month-12 (2 ankle models). The new pipeline was used to create the models. The time needed for this procedure was ~6 hours to generate each ankle model and ~4 days of work for generating the bilateral lower

[1] Best practices suggested at http://simtk-confluence.stanford.edu:8080/display/OpenSim/Simulation+with+OpenSim+-+Best+Practices.

limb model. It is important to highlight, however, that the construction of these models and the results of the repeatability analysis allowed an atlas to be defined, a necessity that will now enable FhG to automate the procedure and significantly reduce the time needed for the manual processing.

5.1 Model generation

The clinical and anthropometric characteristics of the patient under examination are reported in Table 17. Despite a change in body mass, there was no significant variation in body segment lengths during the period of involvement in the study. This allowed the model developed at month-6 to be used as a reference for the models of the other two time points without any adjustment of the body segment lengths. Body mass was adjusted between the three time points to be consistent with the measured variation, but the proportion of mass between the segments was maintained.

Table 13: Anthropometric characteristic of the considered patient at the three time points when data was collected.

	Month 0	Month 6	Month 12
Height [cm]	163	163.6	163.7
Mass [kg]	53.2	63.8	62
Involvement	Both ankles (severe)	None (Inactive disease)	Both ankles (less severe than month-0)

The gait marker registration was performed for each model as described in a previous section.

5.2 Simulations

Once the musculoskeletal models for all time points were produced (Figure 17 A), the standard OpenSim simulation pipeline was performed (Delp et al., 2007). Joint angles were calculated using the OpenSim inverse kinematics tool (Lu and O'Connor, 1999), joint moments using the inverse dynamics analysis (Winter, 2005) and muscle forces estimated using an optimisation technique that minimizes metabolic energy of walking as sum of muscle activation squared (Crowninshield and Brand, 1981; Anderson and Pandy, 2001). Finally, the joint reaction forces were calculated using the analysis (Steele et al., 2012) available in OpenSim.

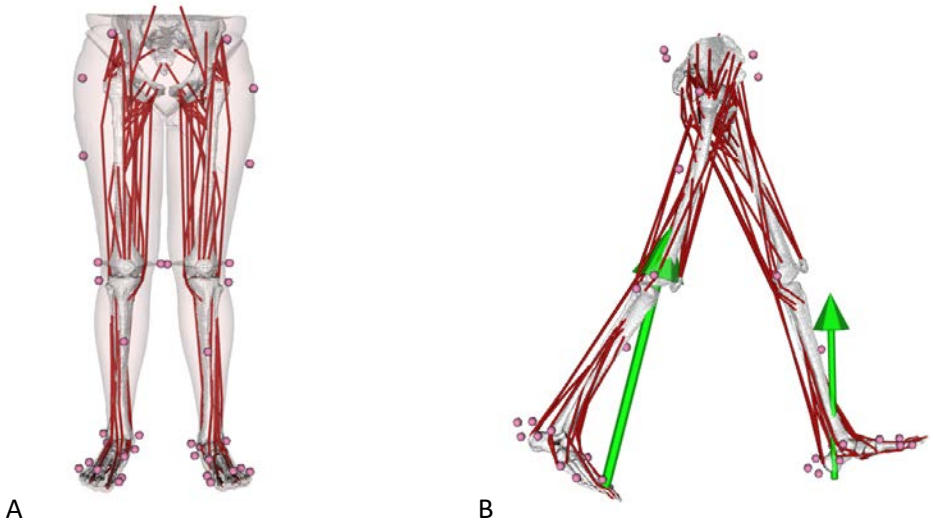

Figure 17: (A) Month-6 models with month-12 patient specific ankles, including virtual markers. (B) A frame of a simulated walking trial.

5.3 Results of the simulations

The inverse kinematics tool was used to calculate the joint angles, and the net joint moments were then computed using the inverse dynamics analysis, the results of which are shown in Figure 18 (where the data are shown for the stance phase only). The results from the inverse dynamics highlight a general trend towards unloading of the hip and knee joints of the right leg, with smaller moments in the right leg at all considered time points. The ankle joint moments, conversely, do not show clear differences between the two simulated sides, although they vary in magnitude between time points. The differences between sides and time points seem to be better highlighted by the resultant ankle joint contact forces, as shown in Figure 19 (magnitude peaks are reported in Table 14). Computed muscle activations are also presented for the month-6 analysis in comparison to normalized EMG signals (Figure 20 and Figure 21) as a tool for indirect validation.

Table 14: Magnitude of the contact forces (mean±standard deviation) acting at the patient ankle at the three time points considered. The number of trials considered in the simulations are specified in brackets.

Ankle side	Ankle peak contact forces [%BW]		
	Month 0	Month 6	Month 12
Right	419±17 (6 trials)	517±18 (7 trials)	466±17 (5 trials)
Left	450±17 (5 trials)	499±18 (6 trials)	481±17 (6 trials)

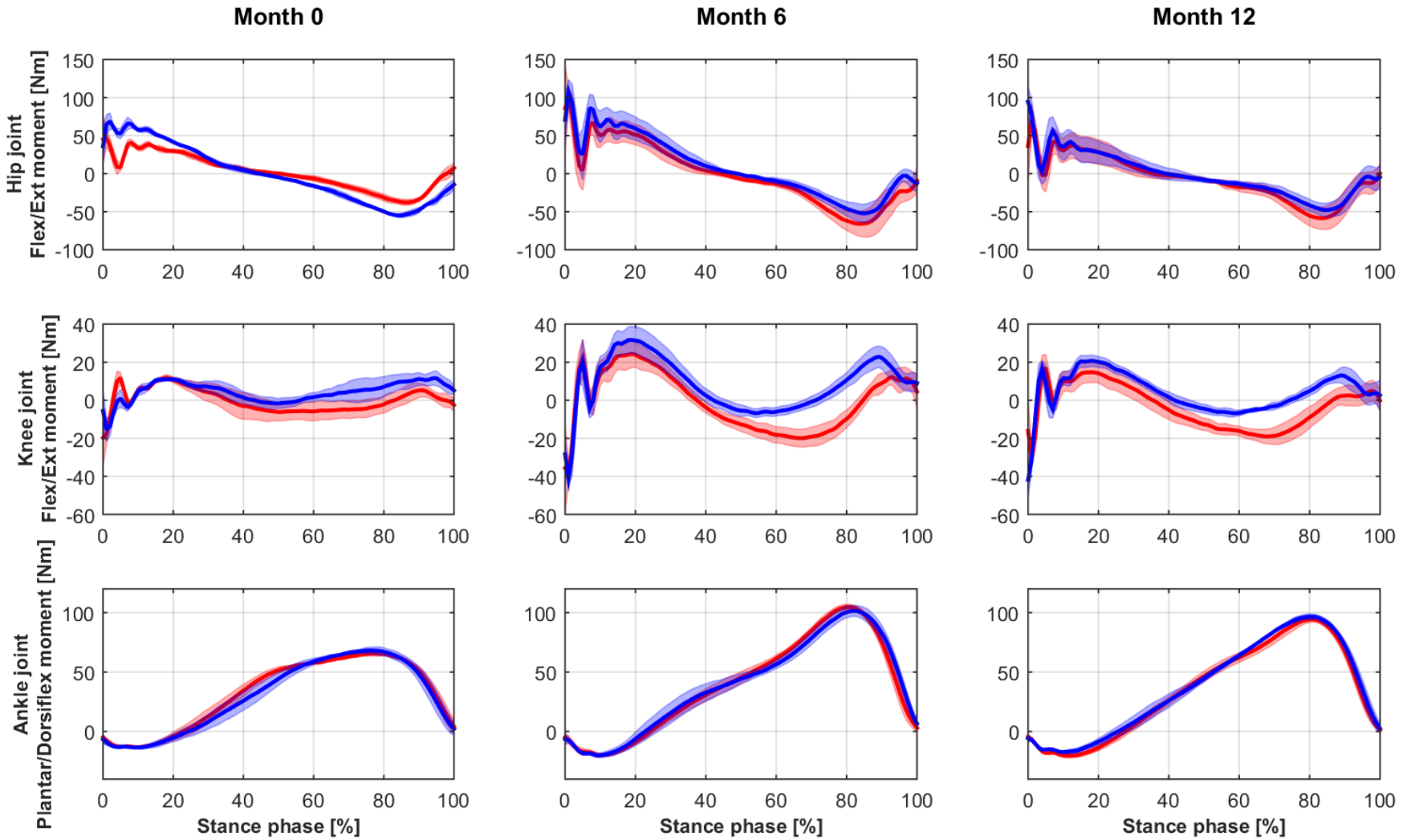

Figure 18: Joint moments in the sagittal plane calculated for the right (red) and left leg (blue) at the three different timepoints (columns).

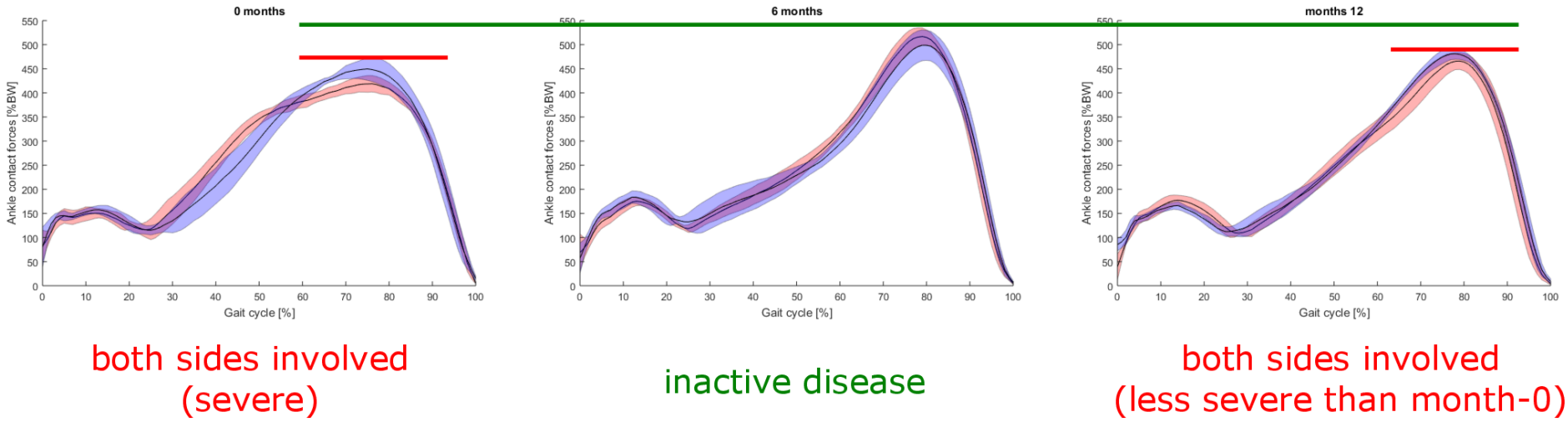

Figure 19: Ankle joint contact forces estimated for right (red) and left (blue) side at the three considered timepoints.

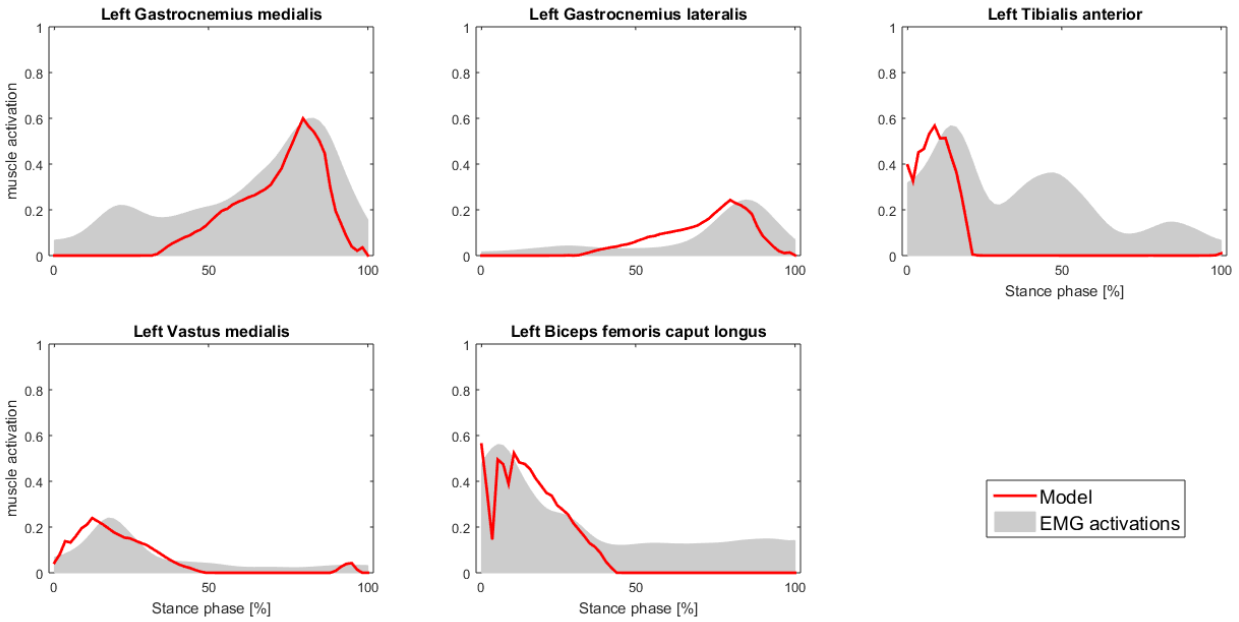

Figure 20: Comparison of EMG signals and computed muscle activation for one walking trial at month-6 (left side).

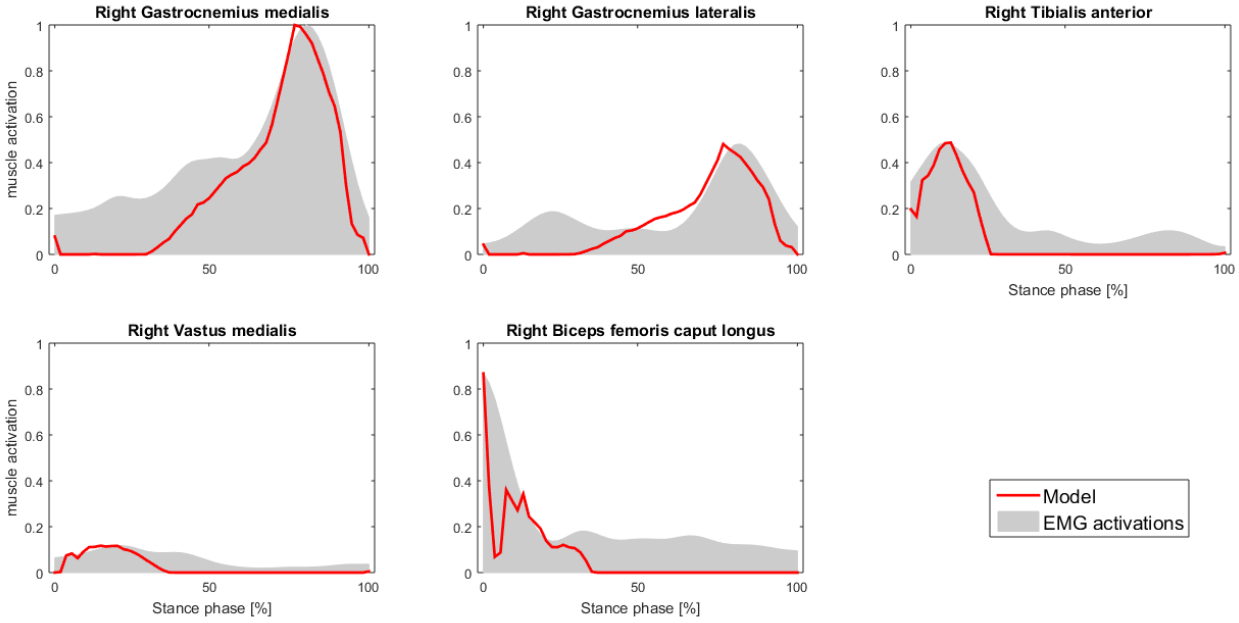

Figure 21: Comparison of EMG signals and computed muscle activation for one walking trial at month-6 (right side).

5.4 Discussion

The simulations presented in this section represent preliminary results obtained for one patient for whom it was possible to model all three time points included in the study. The results are very encouraging, since the

variations of the quantities of interest are consistent with the characteristics of the patient reported by the clinical partners. In particular, joint moment magnitudes are consistent with the clinical situation of the patient at month-0 and month-12. In this patient, in fact, at month-0 both hip, knee, ankle and subtalar joints were involved in the disease, with the lowest joint moments suggesting an overall joint protection strategy, while at month-12 only the knees and ankles were swollen. The intuitive assumption that the patient will load less a painful joint in order to avoid pain seems confirmed by the trend of ankle joint contact forces, which are largest at month-6 (remission) and lowest at month-0 (severe involvement of tibiotarsal and subtalar joints).

An indirect validation of the month-6 model was performed through qualitative comparison of muscle activation (ratio of muscle force over F_{iso}^{m}) against the available EMG signals normalized to the maximum voltage collected on that trial. All major muscles for which the EMG was measured have activation patterns that are well reproduced by the musculoskeletal model, with the exception of *tibialis anterior*. Whereas this aspect needs to be further investigated, the overall agreement between the model activations and the EMG signal patterns gives us confidence that the patient specific modelling techniques developed within this project will be able to suit the purpose of answering the clinical questions at hand.

Future work will focus on generating a larger number of models at different time steps in order to confirm the feasibility of producing biomarkers descriptive of the ankle joint. The minimum level of patient specific elements to introduce in the musculoskeletal model without losing its specificity will also be investigated.

6. Towards a multi-scale model

For applying the muscle forces estimated by the biomechanical model to continuous models of the tibiotalar joint, it is necessary to extract the lines of action of the muscles end express them with respect to the local reference system. A C++ freely available plugin, adapted from the one made available by van Arkel et al. (2013), which allows this operation to be performed in OpenSim was implemented and verified using the Matlab application programming interface (API). The Matlab environment was preferred to C++ as it will give more flexibility for integrating multibody and finite element models.

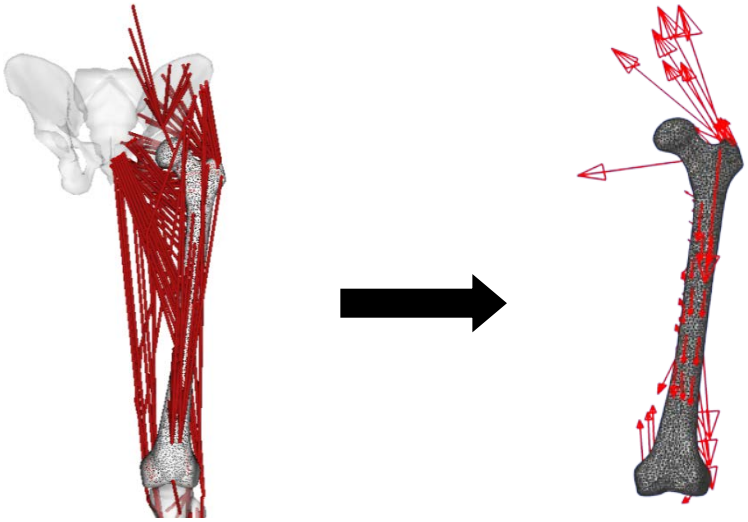

Figure 22 Muscle directions can be extracted from the musculoskeletal model by means of the developed OpenSim plugin and used to define muscle loads on the finite element model.

7. Concluding remarks

This document has outlined significant progresses in data collection, data processing, and modelling. In particular, improvements and refinement of the original anatomical and biomechanical modelling pipelines have been presented, together with an assessment of their reliability.

Data from one patient have been fully processed with the potential of personalised biomechanical models to meaningfully predict the lower limb muscle activations and the joint ankle forces also demonstrated. Future work will focus on large-scale data and model processing, so that patient-specific models are created for each of the enrolled patients. This will be aided by further automation of the image modelling processes.

The focus of the work package for the forthcoming months will also be on advancing multi-scale modelling through the development of finite element models, in order to use the joint reaction forces as loading conditions in the ankle to investigate how the different loads affect cartilage response.

8. References

Anderson, F. and Pandy, M., 2001. Static and dynamic optimization solutions for gait are practically equivalent. Journal of Biomechanics 34, 153 - 161.

Arnold, E., Ward, S., Lieber, R. and Delp, S., 2010. A Model of the Lower Limb for Analysis of Human Movement. Annals of biomedical engineering 38, 269-279.

Besl, P. J. and McKay, N. D., 1992. Method for registration of 3-D shapes. Robotics-DL tentative.
Crowninshield, R. D. and Brand, R. A., 1981. A physiologically based criterion of muscle force prediction in locomotion. Journal of Biomechanics 14, 793-801.

De Groote, F., Van Campen, A., Jonkers, I. and De Schutter, J., 2010. Sensitivity of dynamic simulations of gait and dynamometer experiments to Hill muscle model parameters of knee flexors and extensors. Journal of Biomechanics 43, 1876-1883.

de Leva, P., 1996. Joint center longitudinal positions computed from a selected subset of Chandler's data. Journal of Biomechanics 29, 1231-1233.

Delp, S. L., Loan, J. P., Hoy, M. G., Zajac, F. E., Topp, E. L. and Rosen, J. M., 1990. An interactive graphics-based model of the lower extremity to study orthopaedic surgical procedures. IEEE Transactions on Biomedical Engineering 37, 757-767.

Delp, S. L., Anderson, F. C., Arnold, A. S., Loan, P., Habib, A., John, C. T., Guendelman, E. and Thelen, D. G., 2007. OpenSim: open-source software to create and analyze dynamic simulations of movement. IEEE Transactions on Biomedical Engineering 54, 1940-1950.

Dumas, R., Aissaoui, R., Mitton, D., Skalli, W. and de Guise, J. A., 2005. Personalized body segment parameters from biplanar low-dose radiography. IEEE Transactions on Biomedical Engineering 52, 1756-1763.

Garner, B. A. and Pandy, M. G., 2003. Estimation of Musculotendon Properties in the Human Upper Limb. Annals of biomedical engineering 31, 207-220.

Gordon, A. M., Huxley, A. F. and Julian, F. J., 1966. The variation in isometric tension with sarcomere length in vertebrate muscle fibres. Journal of Physiology 184, 170-192.

Hainisch, R., Gfoehler, M., Zubayer-Ul-Karim, M. and Pandy, M. G., 2012. Method for determining musculotendon parameters in subject-specific musculoskeletal models of children developed from MRI data. Multibody System Dynamics 28, 143-156.

Hill, A. V., 1938. The Heat of Shortening and the Dynamic Constants of Muscle. Proceedings of the Royal Society of London. Series B, Biological Sciences 126, 136-195.

Lloyd, D. G. and Besier, T. F., 2003. An EMG-driven musculoskeletal model to estimate muscle forces and knee joint moments in vivo. Journal of Biomechanics 36, 765-776.

Lu, T. and O'Connor, J., 1999. Bone position estimation from skin marker co-ordinates using global optimisatoin with joint constraints. Journal of Biomechanics 32, 129 - 134.

Manal, K. and Buchanan, T. S., 2004. Subject-Specific Estimates of Tendon Slack Length: A Numerical Method. Journal of applied Biomechanics 20, 195-203.

Modenese, L., Ceseracciu, E., Reggiani, M. and Lloyd, D. G., 2016. Estimation of musculotendon parameters for scaled and subject specific musculoskeletal models using an optimization technique. Journal of Biomechanics 49, 141-148.

Parr, W. C. H., Chatterjee, H. J. and Soligo, C., 2012. Calculating the axes of rotation for the subtalar and talocrural joint using 3D bone reconstructions. Journal of Biomechanics 45, 1103-1107.

Prinold, J. I., Mazzà, C., Di Marco, R., Hannah, I., Malattia, C., Magni-Manzoni, S., Petrarca, M., Ronchetti, A., Tanturri de Horatio, L., van Dijkhuizen, E. H. P., Wesarg, S. and Viceconti, M., 2016. A Patient-Specific Foot Model for the Estimate of Ankle Joint Forces in Patients with Juvenile Idiopathic Arthritis. Annals of biomedical engineering 44, 247-257.

Redl, C., Gfoehler, M. and Pandy, M. G., 2007. Sensitivity of muscle force estimates to variations in muscle–tendon properties. Human Movement Science 26, 306-319.

Scheys, L., Loeckx, D., Spaepen, A., Suetens, P. and Jonkers, I., 2009. Atlas-based non-rigid image registration to automatically define line-of-action muscle models: A validation study. Journal of Biomechanics 42, 565-572.

Scovil, C. Y. and Ronsky, J. L., 2006. Sensitivity of a Hill-based muscle model to perturbations in model parameters. Journal of Biomechanics 39, 2055-2063.

Steele, K. M., DeMers, M. S., Schwartz, M. H. and Delp, S. L., 2012. Compressive tibiofemoral force during crouch gait. Gait & Posture 35, 556-560.

Steger, S., Kirschner, M. and Wesarg, S., 2012. Articulated atlas for segmentation of the skeleton from head & neck CT datasets. 9th IEEE International Symposium on Biomedical Imaging (ISBI). Barcelona, Spain.

Taddei, F., Ansaloni, M., Testi, D. and Viceconti, M., 2007. Virtual palpation of skeletal landmarks with multimodal display interfaces. Informatics for Health and Social Care 32, 191-198.

Thelen, D. G., 2003. Adjustment of Muscle Mechanics Model Parameters to Simulate Dynamic Contractions in Older Adults. Journal of Biomechanical Engineering 125, 70-77.

Valente, G., Pitto, L., Testi, D., Seth, A., Delp, S. L., Stagni, R., Viceconti, M. and Taddei, F., 2014. Are Subject-Specific Musculoskeletal Models Robust to the Uncertainties in Parameter Identification? PLoS ONE 9, e112625.

van Arkel, R. J., Modenese, L., Phillips, A. and Jeffers, J. R., 2013. Hip Abduction Can Prevent Posterior Edge Loading of Hip Replacements. Journal of Orthopaedic Research 31, 1172-1179.

van Sint Jan, S., 2007. Color atlas of skeletal landmark definitions: guidelines for reproducible manual and virtual palpations. Elsevier Health Sciences, ISBN 1455725196.

Ward, S., Eng, C., Smallwood, L. and Lieber, R., 2009. Are Current Measurements of Lower Extremity Muscle Architecture Accurate? Clinical Orthopaedics and Related Research 467, 1074-1082.

Winby, C. R., Lloyd, D. G. and Kirk, T. B., 2008. Evaluation of different analytical methods for subject-specific scaling of musculotendon parameters. Journal of Biomechanics 41, 1682-1688.

Winter, D. A., 2005. Biomechanics and motor control of the human movement. John Wiley & Sons, Waterloo, Ontario, Canada.

Zajac, F. E., 1989. Muscle and tendon: properties, models, scaling, and application to biomechanics and motor control. Critical Reviews in Biomedical Engineering 17, 359-411.

Zatsiorsky, V. M. and Seluyanov, V. N., 1983. The mass and inertia characteristics of the main segments of the human body. In: Matsui, H. and Kobayashy, K. (Eds), Biomechanics VIII-B. Human Kinetics Publishers, Champaign, IL, pp. 1152-1159.

Appendix

Table A.1: Intra- and inter-operator standard deviations (sd) of virtual palpated markers among three repetitions of virtual palpation. Values are tabled for the 22 most repeatable markers included in the final atlas (subset of most repeatable bony landmarks).

	Subject 1		Subject 2		Subject 3	
	intra sd	inter sd	intra sd	inter sd	intra sd	inter sd
shank	(mm)	(mm)	(mm)	(mm)	(mm)	(mm)
trial 1	2.07	2.02	0.73	0.64	0.02	0.18
	0.51	0.47	0.47	0.67	0.74	0.37
	1.06	0.42	0.41	0.60	2.35	2.30
trial 2	1.68	2.79	0.46	0.07	0.14	0.13
	0.34	0.25	0.69	0.32	0.69	0.34
	0.80	1.36	1.79	2.35	0.19	0.76
trial 3	1.80	1.97	0.16	0.45	0.30	0.19
	0.26	0.41	0.28	0.32	0.23	0.74
	0.16	0.32	0.32	0.99	0.69	0.18

	Subject 1		Subject 2		Subject 3	
	intra sd	inter sd	intra sd	inter sd	intra sd	inter sd
talus	(mm)	(mm)	(mm)	(mm)	(mm)	(mm)
trial 1	3.37	3.62	2.27	2.63	0.44	0.56
	1.78	2.69	0.26	1.00	1.65	0.72
	0.30	0.65	0.44	0.42	1.03	1.22
	0.30	0.19	1.46	0.62	1.44	0.92
trial 2	0.48	0.52	0.40	3.86	0.43	0.47
	1.01	1.12	0.87	3.83	0.10	3.12
	0.27	0.43	0.28	0.53	0.60	0.67
	0.19	0.16	1.50	1.83	0.63	0.50
trial 3	0.52	0.94	1.32	2.91	3.62	3.08
	0.08	2.73	3.77	0.24	3.58	2.64
	0.55	0.27	0.38	0.17	0.73	1.12
	0.31	0.39	2.34	2.05	1.18	1.27

	Subject 1		Subject 2		Subject 3	
	intra sd	inter sd	intra sd	inter sd	intra sd	inter sd
hindfoot	(mm)	(mm)	(mm)	(mm)	(mm)	(mm)
trial 1	0.47	1.10	1.61	0.78	0.69	0.80
	0.40	0.66	0.35	0.08	0.80	0.35
	0.77	0.56	0.63	0.76	1.68	3.57
	1.81	0.37	0.94	1.16	0.61	0.84
trial 2	0.03	0.87	0.60	0.70	0.24	0.96
	0.13	0.37	0.17	0.33	0.58	0.30
	0.90	1.06	0.45	0.29	3.53	1.60
	0.25	0.49	0.26	0.63	0.77	0.37
trial 3	0.27	1.06	0.63	1.34	0.71	1.39
	0.16	0.32	0.39	0.19	0.23	1.19
	0.71	0.41	0.57	0.47	2.10	2.22
	0.71	1.03	0.36	0.64	0.15	1.06

	Subject 1		Subject 2		Subject 3	
	intra sd	inter sd	intra sd	inter sd	intra sd	inter sd
forefoot	(mm)	(mm)	(mm)	(mm)	(mm)	(mm)
trial 1	0.34	0.15	0.18	0.41	0.21	1.49
	0.30	0.13	0.02	0.41	1.31	0.71
	0.54	0.28	0.85	0.64	0.25	0.47
	-	-	0.29	0.19	0.12	0.16
	-	-	1.09	1.00	0.12	0.51
	-	-	0.77	0.36	1.54	0.29
trial 2	0.24	0.28	0.91	0.14	0.65	0.31
	0.17	0.36	0.77	0.23	1.33	0.93
	0.25	0.43	0.46	0.48	0.85	0.53
	-	-	0.15	0.14	0.56	0.46
	-	-	0.52	0.96	0.59	0.87
	-	-	0.52	0.55	1.30	1.11
trial 3	0.03	0.25	0.12	0.63	0.73	0.39
	0.27	0.46	0.41	0.27	0.87	0.47
	0.42	0.04	0.70	0.72	0.19	1.29
	-	-	0.51	0.12	0.48	0.35
	-	-	1.53	1.81	0.21	0.45
	-	-	0.44	0.80	0.24	1.34

	Subject 1		Subject 2		Subject 3	
	intra sd	inter sd	intra sd	inter sd	intra sd	inter sd
toes	(mm)	(mm)	(mm)	(mm)	(mm)	(mm)
trial 1	-	-	0.23	0.22	0.23	0.03
	-	-	0.11	0.19	0.29	0.48
	-	-	0.53	1.00	0.46	0.91
	-	-	0.27	0.82	0.67	1.88
	-	-	0.19	0.46	0.31	0.33
trial 2	-	-	0.10	0.28	0.24	0.36
	-	-	0.36	0.25	0.17	0.20
	-	-	1.32	0.92	0.33	0.12
	-	-	0.75	0.03	2.05	0.30
	-	-	0.59	0.34	0.29	0.27
trial 3	-	-	0.10	0.06	0.06	0.10
	-	-	0.15	0.26	0.46	0.17
	-	-	0.12	0.12	0.49	0.41
	-	-	0.15	0.28	0.25	0.67
	-	-	0.83	0.87	0.37	0.35

Table A.2: Mean standard deviations (sd) of palpated markers over 9 performed trials (three operators palpating three time each subject). Low standard deviations (green) mean that the marker is repeatable; high standard deviations (red) mean the marker is not repeatable.

Marker name	Subject 1 sd (mm)	Subject 2 sd (mm)	Subject 3 sd (mm)	mean sd (mm)	notes
TAM	2.66	0.49	0.19	1.11	
post_lat_corner	2.49	1.38	2.36	2.08	deleted
ant_tibia	2.98	1.22	1.27	1.82	deleted
FAL	0.35	0.50	0.56	0.47	
tib_shaft	0.82	1.39	1.41	1.21	*
top_talus	0.96	0.57	0.54	0.69	deleted
lat_process	2.08	2.87	2.00	2.32	needed
med_tub	2.05	2.29	2.30	2.21	needed
post_proc	0.75	0.28	0.73	0.59	
lat_sup	0.47	0.39	0.95	0.60	deleted
post_med	0.24	1.58	1.06	0.96	
STL	0.86	1.90	1.79	1.51	deleted
FCC	0.95	1.11	0.97	1.01	
FNT	1.76	1.18	0.62	1.19	deleted
FGA	3.98	2.11	2.44	2.84	deleted
FPT	0.44	0.32	0.70	0.49	
most_inferior	0.80	4.01	1.06	1.96	deleted
post_inf_cuboid	0.42	1.63	3.11	1.72	deleted
ant_inf_cuboid	0.93	0.49	2.88	1.43	
inf_ant_calc	0.93	0.90	0.97	0.93	deleted
most_ant	0.99	0.75	0.74	0.83	
FMT	0.22	0.47	0.79	0.49	
FM1	0.30	0.44	1.05	0.60	
FM2	0.41	0.59	0.81	0.61	deleted
FM3	0.63	0.37	0.65	0.55	deleted
FM4	0.59	0.63	0.78	0.67	deleted
FM5		0.60	0.80	0.70	
PM4	0.30	0.14	0.30	0.25	deleted
PM3	0.24	0.26	0.39	0.30	deleted
PM2	0.33	0.27	0.31	0.30	deleted
PMT	0.43	0.30	0.41	0.38	
IDM		1.27	0.60	0.93	
IDM2		0.56	0.91	0.74	deleted
IDM3		0.35	1.09	0.72	deleted
IDM4		0.69	1.08	0.89	deleted
IDM5		0.54	1.21	0.88	
D5		0.19	0.19	0.19	
D4		0.11	0.23	0.17	deleted
D3		0.29	0.14	0.21	deleted
D2		0.21	0.21	0.21	deleted
DH		0.21	0.29	0.25	
H_s		0.73	0.51	0.62	
H_i		1.11	0.72	0.92	deleted
H_m		0.51	1.18	0.84	
2_s		0.60	0.44	0.52	deleted
2_i		0.61	0.21	0.41	deleted
3_s		0.85	1.00	0.92	deleted
3_i		0.64	0.41	0.52	deleted
4_s		0.71	0.58	0.64	deleted
4_i		0.53	0.51	0.52	deleted
5_s		0.89	0.36	0.63	deleted
5_i		0.53	0.30	0.41	
5_l		0.14	0.81	0.48	deleted

Table A.3: Intra- and inter-operator standard deviations (sd) of muscular attachments location.

Attachments name	intra sd (mm)	inter sd (mm)	Attachments name	intra sd (mm)	inter sd (mm)	Attachments name	intra sd (mm)	inter sd (mm)
Biceps_long_I	0.37	2.44	Tib_ant_via1	0.24	2.36	EDB5_via2	0.44	1.93
Biceps_short_I	0.37	2.45	Tib_ant_via2	0.94	5.43	FDB4_via	1.87	2.00
Ext_dig_long_O	0.35	2.43	Tib_post_via1	2.87	2.50	EDB4_via2	1.39	1.12
Ext_hal_long_O	0.35	2.40	Gastroc_lat_I	1.19	2.09	EDB5_via1	3.23	4.21
Flex_dig_long_O	0.33	2.44	Gastroc_med_I	2.33	6.33	EDB3_via1	1.82	6.52
Flex_hal_long_O	0.40	2.24	Soleus_I	2.73	2.83	EDB3_via2	0.33	2.32
Gracilis_I	0.32	2.51	Tibialis_post_I	5.13	1.99	EDB4_via1	1.82	4.11
Patella_lig_O	0.27	2.49	EDL_via2	7.22	13.31	FDB3_via	1.32	2.56
Peroneus_brev_O	0.30	9.34	FDL_via2	3.98	1.52	EDB2_via1	1.90	7.33
Peroneus_long_O	0.36	2.39	FDL_via3	0.46	4.09	EDB2_via2	1.33	4.28
Peroneus_tert_O	0.23	2.58	FHL_via2	7.33	1.63	FDB2_via	1.38	1.48
Sartorius_I	0.30	2.49	FHL_via3	3.97	1.32	FHB_via	5.42	4.41
Semimembr_I	0.38	2.50	Per_brev_via3	0.48	1.04	EHB_via	3.30	14.26
Semitendinosus_I	0.32	2.51	Per_long1_via3	1.44	1.33	Ext_dig_long_I	0.65	1.97
Soleus_O	0.34	2.47	EHL_via3	1.23	3.44	Ext_hal_long_I	0.43	0.54
TFL_I	0.30	2.46	Per_long1_via5	2.80	0.67	Flex_dig_long_I	0.80	2.08
Tib_ant_O	0.28	2.43	EDB_O	4.15	5.98	Flex_hal_long_I	0.98	2.86
Tib_post_O	0.33	2.45	EHB_O	4.36	4.87	EDL_via4	1.50	5.83
EDL_via1	0.13	2.88	FDB_O	6.48	3.00	EHL_via6	0.13	1.04
EHL_via1	0.32	2.01	FHB_O	9.59	8.95	FDL_via5	1.94	2.54
EHL_via2	2.03	3.81	Tib_post_via2	9.22	9.20	FDL_via6	0.14	2.76
FDL_via1	3.77	2.47	Per_long1_via4	0.82	2.72	FHL_via5	1.65	3.08
FHL_via1	0.77	6.65	Peroneus_brev_I	0.92	1.28	EHB_I	1.88	0.79
Gracilis_via1	0.36	2.51	Peroneus_long_I	2.89	1.89	EDB2_I	0.89	0.83
Per_brev_via1	1.34	1.16	Peroneus_tert_I	1.90	3.17	EDB3_I	0.51	1.02
Per_brev_via2	0.81	1.07	Tibialis_ant_I	0.52	2.89	EDB4_I	1.15	1.35
Per_long1_via1	0.98	1.23	EHL_via4	4.21	1.14	EDB5_I	0.54	0.94
Per_long1_via2	2.60	1.94	EHL_via5	1.16	1.77	FHB_I	2.45	0.77
Pert_tert_via1	3.02	0.30	FDL_via4	1.85	1.00	FDB2_I	1.81	0.54
Sartor_via2	0.37	2.51	FHL_via4	2.27	4.40	FDB3_I	0.24	1.12
Sartor_via3	0.36	2.51	EDL_via3	4.03	7.43	FDB4_I	0.59	1.42
Semit_via1	0.39	2.50	FDB5_via	3.72	3.64	FDB5_I	0.57	0.26
Tib_ant_via1	0.24	2.36	EDB5_via2	0.44	1.93	FDB5_I	0.57	0.26

Table A.4: Standard deviations (sd) between operators' virtual palpations of the muscular attachments. Green (low sd) to red (high sd) color bar simplifies the identification.

Attachments name	Subject 1 sd (mm)	Subject 2 sd (mm)	Subject 3 sd (mm)	mean sd (mm)	Attachments name	Subject 1 sd (mm)	Subject 2 sd (mm)	Subject 3 sd (mm)	mean sd (mm)
Biceps_long_I	0.86	2.44	2.01	1.77	EHB_O	6.11	5.98	8.82	6.97
Biceps_short_I	0.86	2.45	2.03	1.78	EDB_O	13.69	4.87	5.57	8.04
Ext_dig_long_O	0.76	2.43	2.02	1.74	FDB_O	4.12	3.00	0.51	2.54
Ext_hal_long_O	0.70	2.40	1.93	1.68	FHB_O	16.99	8.95	1.14	9.03
Flex_dig_long_O	0.45	2.44	2.08	1.66	Tib_post_via2	10.23	9.20	4.24	7.89
Flex_hal_long_O	0.24	2.24	1.44	1.31	Per_long1_via4	1.44	2.72	0.81	1.66
Gracilis_I	0.94	2.51	2.46	1.97	Peroneus_brev_I	4.94	1.28	1.66	2.63
Patella_ligam_O	1.25	2.49	2.64	2.12	Peroneus_long_I	4.14	1.89	1.85	2.63
Peroneus_brev_O	5.43	9.34	1.27	5.34	Peroneus_tert_I	0.74	3.17	2.61	2.17
Peroneus_long_O	0.84	2.39	1.87	1.70	Tibialis_ant_I	3.22	2.89	3.32	3.14
Peroneus_tert_O	3.52	2.58	1.46	2.52	EHL_via4	1.64	1.14	2.98	1.92
Sartorius_I	0.90	2.49	2.50	1.96	EHL_via5	1.01	1.77	2.67	1.82
Semimembr_I	1.34	2.50	2.24	2.03	FDL_via4	1.81	1.00	1.47	1.43
Semitendinosus_I	0.87	2.51	2.43	1.94	FHL_via4	3.59	4.40	1.88	3.29
Soleus_O	0.77	2.47	2.22	1.82	EDL_via3	2.75	7.43	2.55	4.24
TFL_I	1.55	2.46	2.39	2.13	FDB5_via	2.94	3.64	1.38	2.65
Tib_ant_O	1.30	2.43	2.34	2.02	EDB5_via2	1.52	1.93	0.67	1.37
Tib_post_O	0.74	2.45	2.16	1.78	FDB4_via	0.76	2.00	2.85	1.87
EDL_via1	7.63	2.88	12.30	7.60	EDB4_via2	0.99	1.12	0.92	1.01
EHL_via1	9.14	2.01	1.59	4.25	EDB5_via1	5.25	4.21	3.99	4.48
EHL_via2	5.03	3.81	5.24	4.69	EDB3_via1	1.85	6.52	0.99	3.12
FDL_via1	6.94	2.47	8.37	5.93	EDB3_via2	1.89	2.32	1.37	1.86
FHL_via1	1.62	6.65	2.30	3.52	EDB4_via1	3.11	4.11	4.15	3.79
Gracilis_via1	1.47	2.51	2.36	2.11	FDB3_via	1.04	2.56	1.02	1.54
Per_brev_via1	1.97	1.16	0.71	1.28	EDB2_via1	6.43	7.33	2.47	5.41
Per_brev_via2	2.02	1.07	2.21	1.77	EDB2_via2	2.53	4.28	1.03	2.61
Per_long1_via1	0.52	1.23	1.25	1.00	FDB2_via	0.91	1.48	1.41	1.26
Per_long1_via2	1.70	1.94	2.26	1.97	FHB_via	3.36	4.41	2.31	3.36
Pert_tert_via1	7.85	0.30	4.48	4.21	EHB_via	3.25	14.26	3.36	6.96
Sartor_via2	1.73	2.51	2.34	2.19	Ext_dig_long_I	6.70	1.97	0.40	3.02
Sartor_via3	1.36	2.51	2.35	2.07	Ext_hal_long_I	0.83	0.54	0.30	0.56
Semit_via1	1.46	2.50	2.21	2.06	Flex_dig_long_I	1.41	2.08	1.50	1.66
Tib_ant_via1	1.57	2.36	2.34	2.09	Flex_hal_long_I	0.98	2.86	2.05	1.96
Tib_ant_via2	0.69	5.43	11.82	5.98	EDL_via4	1.75	5.83	2.26	3.28
Tib_post_via1	3.42	2.50	7.96	4.63	EHL_via6	1.84	1.04	1.91	1.60
Gastroc_lat_I	2.64	2.09	1.56	2.10	FDL_via5	2.29	2.54	1.92	2.25
Gastroc_med_I	5.36	6.33	3.23	4.97	FDL_via6	2.03	2.76	3.88	2.89
Soleus_I	2.63	2.83	0.55	2.00	FHL_via5	0.69	3.08	0.87	1.54
Tibialis_post_I	0.60	1.99	3.53	2.04	EHB_I	0.69	0.79	1.41	0.96
EDL_via2	10.77	13.31	2.79	8.96	EDB2_I	4.54	0.83	2.06	2.48
FDL_via2	4.89	1.52	0.86	2.42	EDB3_I	3.24	1.02	0.97	1.74
FDL_via3	0.41	4.09	10.83	5.11	EDB4_I	2.06	1.35	0.46	1.29
FHL_via2	1.91	1.63	7.77	3.77	EDB5_I	2.07	0.94	0.64	1.21
FHL_via3	5.43	1.32	5.27	4.01	FHB_I	1.63	0.77	0.72	1.04
Per_brev_via3	5.97	1.04	0.48	2.50	FDB2_I	1.89	0.54	1.64	1.36
Per_long1_via3	5.27	1.33	5.09	3.89	FDB3_I	2.61	1.12	1.80	1.84
EHL_via3	3.60	3.44	4.60	3.88	FDB4_I	1.52	1.42	2.31	1.75
Per_long1_via5	5.13	0.67	3.22	3.01	FDB5_I	1.35	0.26	2.38	1.33